DTP/95/68
LU TP 95–18
August 1995

QED Interconnection Effects on W Momentum Distributions at LEP 2

Valery A. Khoze
Department of Physics, University of Durham,
Durham, DH1 3LE, U.K.

and

Torbjörn Sjöstrand
Department of Theoretical Physics 2, University of Lund,
Sölvegatan 14A, S-223 62 Lund, Sweden

Abstract

The process $e^+e^- \to W^+W^- \to f_1\bar{f}_2\,f_3\bar{f}_4$ contains charges in the initial, intermediate and final stages. This gives a rich selection of possible QED interconnection effects. Coulomb interaction is the simplest of these, and can thus be used to explore consequences. We study a number of experimental observables, with emphasis on those related to the W momentum distribution. Second-order Coulomb effects are shown to be practically negligible. The limited LEP 2 statistics will not allow detailed tests, so any theory uncertainty will be reflected in the systematic error on the W mass. Currently the uncertainty from this source may be as high as 20 MeV.

1 Introduction

A precision measurement of the W-boson mass $M_{\rm W}$ is one of the main objectives of the LEP 2 e^+e^- collider. To exceed the precision of $\overline{\rm p}$p collider experiments, $M_{\rm W}$ should be measured to an accuracy of 50 MeV or better, see e.g. ref. [1]. The success of such an ambitious goal relies on an accurate theoretical knowledge of the dynamics of the production and decay stages in $e^+e^- \to W^+W^- \to 4$ fermions. Moreover, owing to the large W width $\Gamma_{\rm W}$, these stages are not independent but may be interconnected by QED and QCD interference effects, which also must be kept under precise theoretical control. Interconnection phenomena may efface the separate identities of the two W bosons, and the final state may no longer be considered as a superposition of two separate W decays. All such effects related to the radiatively corrected (total and differential) W^+W^- production cross section should be accurately calculated, so that the W mass can be extracted from data.

For the totally inclusive W^+W^- production cross section there is a general proof [2, 3] (also [4]) that the radiative interconnection effects are suppressed by $O(\alpha\Gamma_{\rm W}/M_{\rm W})$ or $O(\alpha_{\rm s}^2\Gamma_{\rm W}/M_{\rm W})$. The only exception is the Coulomb interaction between two slowly moving W's, which is modified by the instability effects in the very narrow region just near threshold, $\sqrt{s}-2M_{\rm W} \lesssim \Gamma_{\rm W}$. By contrast, differential distributions could be distorted on the level of $O(\alpha)$ or $O(\alpha_{\rm s}^2)$. (Analogous QCD final-state interaction effects appear in the differential distributions of $t\bar{t}$ production processes [3, 4, 5, 6, 7].) These distortions should vanish in the zero-width limit. In ref. [8] we studied the possible impact of QCD interconnection (colour rearrangement) effects for the direct reconstruction of the W mass from the hadronic decay products (as favoured by experimenters [9]). The limited understanding on the hadronization of overlapping hadronic systems was shown to imply a systematic error on $M_{\rm W}$ of 30–40 MeV. Additional errors could come from Bose-Einstein effects among the final-state hadrons [10, 11].

There are also purely QED final-state interactions, however, that can produce non-factorizable radiative corrections to the Born cross section of $e^+e^- \to W^+W^- \to 4$ fermions [12, 3]. Specifically, there is a class of virtual interference effects corresponding to the so-called charged-particle poles [3, 4, 13], which induce an explicit dependence of the differential cross section on the W-boson virtualities. This is related to the fact that the dominant contribution to the non-factorizable radiative interferences comes from sufficiently soft photons with $k_\gamma \lesssim \Gamma_{\rm W}$. The phenomenon could be exemplified by the Coulomb interaction between two unstable W bosons [2, 14] (also [15]). (To the best of our knowledge, the necessity to take into account the effects of Coulomb final-state interactions on the W momentum distribution was first pointed out in ref. [8].) Coulomb terms could be uniquely separated from the other electroweak corrections in the threshold region, where they provide the dominant source of the off-shellness effects.

Other radiative mechanisms may become essential at larger W-boson velocities β, for example, those caused by the intermediate–final or final–final interferences [3, 13]. (We recall, however, that the Coulomb correction is not uniquely defined and gauge independent in the relativistic region.) In the ultrarelativistic region it is expected [13] that the dependence on the W virtuality disappears in the full expression for radiative corrections. This phenomenon is deeply rooted in the conservation of a charged current.

In the threshold region the Born cross section depends strongly on the momentum p of the unstable particle. This leads to a competition between the Breit-Wigner factors and the rest of the cross section ($\propto \beta$) [8], which induces a significant change between the

nominal and the actual average mass. In the energy range

$$M_{\mathrm{W}} \gg E \geq \Gamma_{\mathrm{W}} \ , \tag{1}$$

where $E = \sqrt{s} - 2M_{\mathrm{W}}$ is the nonrelativistic energy of the two W's, the mass shift towards lower values is of $O(\Gamma_{\mathrm{W}}^2/E)$. This shift changes sign at around 190 GeV because of the increasing rôle of the negative higher-order terms ($\propto \beta^2$) in the Born cross-section expression [16].

Our interest is in the dynamical QED effects, on top of the purely kinematical distortions. The Coulomb final-state interaction between unstable W's could, in principle, induce a systematic shift in the reconstructed M_{W} of $O(\alpha\pi\Gamma_{\mathrm{W}})$ [14, 16] that is of the same magnitude as the aimed-for precision of LEP 2 measurements. Therefore the shifts in the W momentum distribution is the result of a complicated interplay between phase-space and virtuality-induced effects appearing in the radiatively corrected cross section for $\mathrm{e^+e^-} \to \mathrm{W^+W^-} \to 4$ fermions. In the main region of LEP 2 running, $\sqrt{s} \simeq 175$ GeV, the two effects above are of the same order. To obtain reliable numerical results one also needs to analyze carefully the rôle of other final-state interaction mechanisms (for such an attempt see ref. [13]).

In this paper we analyze the impact of QED interconnection, exemplified by the Coulomb effects on the W momentum distribution in the threshold region. This region is relevant for LEP 2 physics, and it is just here that off-shell and finite-width effects are most important [2, 3, 14, 17]. It may be seen as a continuation of the studies presented for mass distributions in ref. [16].

Particular emphasis is put on the momentum distribution of the W's. This is especially relevant since the Coulomb effects depend primarily on the W momentum. However, there is also an experimental reason for such a choice. In the best of possible worlds, the final state could be subdivided into two sets of particles, one stemming from the $\mathrm{W^+}$ decay and the other from the $\mathrm{W^-}$. The invariant masses m_1 and m_2 could then be calculated and directly compared with theory. In addition to the assignment problems already mentioned, such an approach suffers from the limited energy resolution of detectors. Jet directions, on the other hand, are much better reconstructed. If energy and momentum conservation relations can be used, i.e. if jet energies are suitably rescaled to the known $\mathrm{e^+e^-}$ beam energy, the W mass is better constrained [9]. Optimal use is made of the experimental information if the $\mathrm{W^+}$ and $\mathrm{W^-}$ of each event are assumed to have the same mass, i.e. if one single average mass $\overline{m}$ is extracted for each event, rather than m_1 and m_2 separately. Such a mass measurement obviously is equivalent to a momentum measurement, according to the relation $\sqrt{s} = 2\sqrt{\overline{m}^2 + p^2}$. However, the momentum is the more direct observable, since it is related to the acollinearity of the jet pairs; we recall that the limit $p = 0$ corresponds to each hadronic W decay giving a pair of back-to-back jets. A measurement along these lines is therefore excluded only when both W's decay leptonically.

The results presented here are aimed at the rather modest task of evaluating the size of the QED interconnection effects. They should only be considered as a qualitiative guide rather than a complete numerical prediction. In what we follows, incoming electrons and positrons are assumed unpolarized, and initial-state radiation (ISR) effects are neglected. We also assume that all particles can be perfectly well measured and neglect the QCD interconnection effects.

In section 2 some of the basic Coulomb formulae are reviewed, with emphasis on the physical origin and consequences. Section 3 contains a numerical study of several observables relevant at LEP 2, with conclusions on the practical importance of Coulomb

effects, on the impact of theoretical uncertainties, and on the choice of experimental observables. Finally, section 4 contains a summary and an outlook.

2 Qualitative discussion

For illustrative purposes we present here the results for momentum distributions in the non-relativistic approximation. The numerical calculations in the next section, however, are based on the full relativistic formulae of ref. [14].

As shown in ref. [7] (see also ref. [14]) the non-relativistic Green's function describing the interaction of the W's depends only on one off-shell variable, namely the W momentum p ($p = |\mathbf{p}^+| = |\mathbf{p}^-|$ in the rest frame of the pair). The integration over the $\mathrm{W}^\pm$ squared masses s_1 and s_2 reduces to an integration over p^2 with

$$p^2 = \frac{(s - s_1 - s_2)^2 - 4 s_1 s_2}{4s} \simeq (\sqrt{s} - \sqrt{s_1} - \sqrt{s_2}) M_{\mathrm{W}} \ . \tag{2}$$

In the dominant p region the differential distribution for $\mathrm{e^+e^-} \to \mathrm{W^+W^-} \to \mathrm{f_1\bar{f}_2\, f_3\bar{f}_4}$ can be written in terms of the rapidly changing variable

$$x = \frac{M_{\mathrm{W}} E - p^2}{M_{\mathrm{W}} \Gamma_{\mathrm{W}}} \tag{3}$$

as

$$\frac{1}{B(\mathrm{W^+} \to \mathrm{f_1\bar{f}_2})\, B(\mathrm{W^-} \to \mathrm{f_3\bar{f}_4})} \frac{\mathrm{d}\sigma}{\mathrm{d}x} = \frac{\sigma_0}{\pi} \frac{1}{1 + x^2} \left[\left(1 + \frac{\alpha}{\pi} \delta_{\mathrm{H}} \right) + \frac{\alpha}{\beta} \overline{\delta}_{\mathrm{C}} \right] \ , \tag{4}$$

with $\beta = 2p/\sqrt{s}$. Here δ_{H} is the so-called hard correction and $\alpha\overline{\delta}_{\mathrm{C}}/\beta$ is the first-order Coulomb term [2, 14],

$$\overline{\delta}_{\mathrm{C}} = \frac{\pi}{2} - \arctan \frac{|\kappa|^2 - p^2}{2 p p_1} \ , \tag{5}$$

with

$$\kappa = \sqrt{-M_{\mathrm{W}}(E + i\Gamma_{\mathrm{W}})} \equiv p_1 - i p_2 \ . \tag{6}$$

For a complete calculation, one must add to eq. (4) the contributions from other final-state interconnection terms.

For the energy region (1) one finds

$$\overline{\delta}_{\mathrm{C}} = \frac{\pi}{2} - \arctan x \ . \tag{7}$$

In this region p_1 and p_2 have very transparent interpretatations:

$$R_\tau \sim \frac{1}{p_1} \sim \frac{\beta_0}{\Gamma_{\mathrm{W}}} \tag{8}$$

(with $\beta_0 = p_0/M_{\mathrm{W}} \simeq \sqrt{E/M_{\mathrm{W}}}$) is the typical spatial separation between the diverging quasi-stable W's, while

$$R_{\mathrm{C}} \sim \frac{1}{p_2} \sim \frac{1}{p_0} \sim \frac{1}{|\kappa|} \tag{9}$$

is the characteristic distance of the Coulomb interaction between on-mass-shell W bosons. Thus the dominant contribution to $\overline{\delta}_{\mathrm{C}}$ comes from values $r \lesssim 1/p_0$, where

$p_0 = \sqrt{s/4 - M_W^2}$ and r is the relative distance between the W's, as discussed in detail in ref. [14]. $\overline{\delta}_C$ depends crucially on the virtuality, and is controlled by the phase shift between the spatial oscillations corresponding to the actual momentum p and the characteristic momentum p_2. Let us briefly discuss the main messages of an analysis of this momentum distribution.

1. For stable W's the on-the-mass-shell Coulomb term would always induce a shift of the distribution towards lower momentum values. In this limit, the exact Coulomb result [18] is actually twice the first-order contribution ($\pi/2$ in eq. (5)).
2. For unstable W's $\overline{\delta}_C$ is always below the on-the-mass-shell value of $\pi/2$ for $p < |\kappa|$ and exceeds it for $p > |\kappa|$. The transition occurs dominantly when

$$|p - p_2| \lesssim p_1 \ . \tag{10}$$

   For region (1) this corresponds to $|x| \lesssim 1$. When $p < p_0$ the effects of destructive interference accumulate in the course of integration over distances r up to [14]

$$r \lesssim \frac{1}{p - p_0} < \frac{\beta_0}{\Gamma_W} \tag{11}$$

   and, as a result, $\overline{\delta}_C$ gets screened. Correspondingly, when $p > p_0$, there is a constructive interference in the same range of r values, leading to an increase of $\overline{\delta}_C$.
3. In the formal limit $M_W \gg |\kappa| \gg p$ one has

$$C = \frac{\alpha}{\beta}\overline{\delta}_C \simeq \alpha \frac{2p_1}{\sqrt{E^2 + \Gamma_W^2}} \ . \tag{12}$$

   Contrary to the stable case, the Coulomb correction C does not blow up at $\beta \to 0$ but reaches its maximal value of $\alpha\sqrt{2M_W/\Gamma_W}$ at $E = 0$. Below threshold, when $|E| \gtrsim \Gamma_W$,

$$C \simeq 2\alpha \sqrt{\frac{M_W}{|E|}} \ . \tag{13}$$

   In region (1), relevant for LEP 2, Coulomb corrections are suppressed,

$$C \simeq \frac{\alpha}{\beta_0} \frac{\Gamma_W}{E} \ . \tag{14}$$

   The screening of the $1/p$ singularity for $p \ll p_0$ also takes place for higher-order Coulomb effects. This can be explicitly seen from the general formulae presented in ref. [14]. The higher-order Coulomb terms could in principle be more important numerically for differential distributions than for the total cross section; see however the discussion in the next section.
4. $\overline{\delta}_C \to \pi$, i.e. twice the leading-order on-the-mass-shell result, when $M_W \gg p \gg |\kappa|$. However, when $E \gg \Gamma_W$ and $M_W \gg p \gg p_0$ the Coulomb correction $\alpha\pi/p$ formally is much smaller than the on-the-mass-shell value $\alpha\pi/(2p_0)$. In region (1) the arctan modification of $\overline{\delta}_C$ in eq. (7) is an odd function of x, so after integration over p the total cross section agrees with the stable-W result.

The instability effects induced by Coulomb interactions are expected to be reduced at relativistic energies because of the contributions of other final-state interaction mechanisms. We will return to this issue below.

3 Numerical results

In the following calculations, we assume a W mass $M_{\mathrm{W}} = 80.41$ GeV, based on the recent CDF number [19], so as to simplify comparisons with the results of ref. [16]. The width is then $\Gamma_{\mathrm{W}} = 2.1$ GeV. Results are presented in the energy range 150–200 GeV, and for six discrete energies: 10 GeV and Γ_{W} below threshold, at threshold, Γ_{W} above threshold, at 175 GeV (typical LEP 2 running energy) and 30 GeV above threshold. Initial-state photon radiation is neglected, so as not to confuse the issue — in an idealized world this would be obtained by the process $\gamma\gamma \to \mathrm{W^+W^-}$. Other interfering graphs, such as $\mathrm{e^+e^-} \to \mathrm{Z^0Z^0} \to 4$ fermions, are not considered. Only trivial loop corrections are included, such as the running of α and α_{s}. The lowest-order cross section σ_0 is therefore given by the Muta et al. expression [20].

Several comparisons will be presented between alternative descriptions of Coulomb effects. This will help us assess the impact of QED interconnection, and to estimate uncertainties.

- The simplest possible alternative is to have no Coulomb corrections at all, henceforth designated "no Coulomb". Many studies in the past have been based on this approach, i.e. using σ_0 unmodified.
- In the first-order "stable Coulomb" description, the two W bosons are considered as stable particles. Then σ_0 is modified by a simple factor $1 + \alpha\overline{\delta}_{\mathrm{C}}/\beta = 1 + \pi\alpha/2\beta$.
- The "unstable Coulomb" approach is a realistic standard for the effects of unstable W's. Again the multiplicative factor is $1 + \alpha\overline{\delta}_{\mathrm{C}}/\beta$, but now $\overline{\delta}_{\mathrm{C}}$ is given by eq. (5).
- Recently simple formulae were presented for the calculation of the Coulomb effects for unstable W's to second order [21], "second-order Coulomb". The cross section is now given by σ_0 multiplied by a factor $|f(\mathbf{p}, E)|^2$, with

$$f(\mathbf{p}, E) = 1 + \frac{\alpha\sqrt{s}}{4ip} \ln D + \frac{\alpha^2 s}{16ip\kappa} \int_0^1 \frac{\mathrm{d}z}{z} \ln \frac{1 + zD}{1 + z/D} \ , \tag{15}$$

  where $D = (\kappa + ip)/(\kappa - ip)$ and κ is defined in eq. (6).

Fig. 1 compares the total $\mathrm{e^+e^-} \to \mathrm{W^+W^-}$ cross section in the four scenarios above as a function of c.m. energy. The differences are more readily visible in Fig. 2, where the cross sections have been normalized to the no-Coulomb one. The corrections reach a maximum at around threshold, of about 6%, and thereafter drop, asymptotically like $1/\beta_0$. They also drop below threshold. This latter behaviour may be understood from the shape of the differential momentum distribution $\mathrm{d}\sigma/\mathrm{d}p$ in the four scenarios above, Fig. 3. Note the very broad momentum spectra at energies below the threshold, where (at least) one of the W's is pushed significantly off the mass shell, and thus has a wide mass distribution. This depletion of the low-β region thus reduces the Coulomb corrections below threshold. Above threshold the spectrum is peaked close to the on-mass-shell value p_0 with a width decreasing like $\delta p \sim M_{\mathrm{W}}\Gamma_{\mathrm{W}}/p_0$.

As above, differences between the alternative Coulomb scenarios are more easily seen it the ratio of $\mathrm{d}\sigma/\mathrm{d}p$ distributions with and without Coulomb effects included, Fig. 4. In particular note the characteristic destructive interference for $p < p_0$ in the unstable Coulomb case.

Even with this expanded scale, the difference between first- and second-order unstable Coulomb is very small. To further quantify effects, Fig. 5 gives the ratio of the second-order contribution to the first-order one. At energies below and around threshold, the effects are positive but only a few per cent, and vary slowly with p. Above threshold, the

difference between low and high p is noticeable on this scale. For $p > p_0$ the effects are close to vanishing, $< 1\%$, but become negative of $O(10\%)$ for for $p < p_0$. In the limit $p \ll p_0$ a simplified analytical expression is

$$|f(\mathbf{p}, E)|^2 = 1 + \frac{2\alpha M_{\mathrm{W}} p_1}{|\kappa|^2} \left\{ 1 + \frac{\alpha M_{\mathrm{W}}}{2p_1} \left[1 + 2 \ln 2 \frac{p_1^2 - p_2^2}{|\kappa|^2} \right] \right\} . \tag{16}$$

This gives a ratio indicated by a dashed line in Fig. 5. The sign of the second-order effect is such as to further reduce the next-to-vanishing first-order Coulomb corrections for $p < p_0$. We must therefore conclude that it will be impossible to observe any second-order Coulomb effects in the differential distributions at LEP 2. This alternative will largely be dropped from the continued discussion, although it is included in the figures.

As noted earlier, the contributions of other intermediate–final and final–final interaction mechanisms have been neglected in the above scenarios, either the calculation is first- or second-order. Driven by physical intuition we might try to estimate the possible impact of such screening corrections by using a simplified formulae containing an extra factor $(1-\beta)^2$ in front of the arctan term in eq. (5) of the first-order unstable Coulomb formulae, "dampened Coulomb". This is in agreement with the results of ref. [13], where an attempt is made to perform the quantitative studies of the instability effects in the relativistic region. However, it should be noted that the asymptotic behaviour does not constrain the form for LEP 2 energies, where $\beta \simeq 1/2$, and thus the numerical difference between two asymptotically equivalent forms such as $(1-\beta)^2$ and $(1-\beta^2)^2$ (or $(1-\beta)^2$ and $(1-\beta_0)^2$) is very large. The curves for this alternative at 175 and 190 GeV in Fig. 4 should therefore be taken as a trial only.

The ansatz above gives a Coulomb effect that is essentially constant as a function of p. Around p_0 the sharp increase noted in the unstable Coulomb case is considerably dampened, since $(1-\beta)^2 \sim (1-0.5)^2 = 0.25$. The visual impression is of an even stronger dampening than just a factor 4, since the general $1/\beta$ fall-off comes in addition and is common. Formally, the dampened Coulomb option can be seen as a mixture of $(1-\beta)^2$ parts of the unstable Coulomb and $1-(1-\beta)^2$ of the stable Coulomb, which offers an alternative approach to understanding the rôle of the $1/\beta$. Since the fraction of the stable Coulomb vanishes like $2\beta - \beta^2$ for $\beta \to 0$, but the Coulomb factor increases like $1/\beta$, the flat behaviour for small p is to be expected. This should not be given too much emphasis, however, since we already noted that the whole approach is unreliable for the LEP 2 energy region and in particular for momenta that deviate too much from p_0. However, in summary, it must be concluded that the dampened Coulomb scenario looks rather much like the no-Coulomb ones, except that the cross section is larger. So long as we are only concerned with distributions normalized per event, no separate figures need therefore be given for this alternative. This conclusion is not valid around or below threshold, but numerically is a sensible approximation from 170 GeV onwards.

We now proceed to quantify how much event properties are changed by Coulomb effects. Fig. 6 shows the average W momentum as a function of c.m. energy. At large energies this is increasing like $\langle p \rangle \approx \sqrt{s/4 - M_{\mathrm{W}}^2}$, but around threshold one or both W's are pushed off mass shell and so $\langle p \rangle$ stabilizes at a level around 20 GeV. The addition of Coulomb effects gives a shift of around 120 MeV in the threshold region, Fig. 7. The effect is here negative, i.e. the Coulomb factors enhance the low-momentum tail of the spectrum (cf. Fig. 4), giving a reduced $\langle p \rangle$. From 164 GeV onwards the destructive interference at low momenta leads to a net $\langle p \rangle$ shift upwards in the unstable Coulomb case. Lower momenta are always favoured for the (unrealistic) stable Coulomb alternative, so the

asymptotic convergence towards the no-Coulomb baseline is from opposite directions for a description in terms of stable or unstable W bosons.

Fig. 8 shows the shift between the average W mass of events and the nominal M_{W} mass parameter (cf. ref. [16]). Around and below threshold this is a negative number, while it becomes positive at around 190 GeV. This is explained as a combination of phase space and cross section effects, as discussed in the introduction. Coulomb effects on the average W mass $\langle m \rangle$ are opposite in sign and about half as large as those on the average W momentum $\langle p \rangle$, Fig. 9. This is easily understood from the relation $p^2 + m^2 \approx s/4 \Longrightarrow \delta m \approx -p\delta p/m$, where $1/4 \lesssim \langle p \rangle / m \lesssim 3/4$ for the energy range considered here. The mass difference betweem first- and second-order Coulomb effects is seen to be below 3 MeV everywhere, i.e. completely negligible.

Since each event contains two W's, it is possible to study separately the mass distribution of the lighter and the heavier W of each events. Figs. 10 and 11 show the Coulomb effects on the average light and heavy mass, $\min(m_1, m_2)$ and $\max(m_1, m_2)$. Below and around threshold almost the whole W mass shift is found in the lighter W: since the lighter W here is off the mass shell, a further change of the mass means a smaller relative change of the propagator value than a corresponding change for the heavier W. Mathematically, a W propagator $\rho \simeq 1/((s - M_{\mathrm{W}}^2)^2 + M_{\mathrm{W}}^2\Gamma_{\mathrm{W}}^2)$ gives a relative change $(1/\rho)|\mathrm{d}\rho/\mathrm{d}s| = 2|s - M_{\mathrm{W}}^2|/((s-M_{\mathrm{W}}^2)^2 + M_{\mathrm{W}}^2\Gamma_{\mathrm{W}}^2)$ that is maximal around $\sqrt{s} \simeq M_{\mathrm{W}} \pm \Gamma_{\mathrm{W}}/2$ and falls off like $1/|s - M_{\mathrm{W}}^2|$ in either tail. At larger energies the mass shift is shared evenly between the two W's, which here both are about equally close to the nominal mass M_{W}.

In the threshold region, there would then be two reasons to base a topological determination of the W mass on the mass distribution of the heavier W of the event. Firstly, Coulomb corrections are small, and therefore also the associated uncertainty. Secondly, this mass distribution is significantly narrower that that of the lighter W or even that of the average mass $(m_{\mathrm{heavy}} + m_{\mathrm{light}})/2$, Figs. 12, 13 and 14, so the statistical error would be smaller. However, there are also two reasons against such a study. Firstly, it would be a major experimental challenge to reconstruct two W masses per event, so the loss in accuracy from experimental effects would almost certainly outweight the above gain. Secondly, in this energy region a better accuracy can be obtained from a measurement of the total cross section [1].

The root-mean-square width of the average W mass distribution is narrowest at around 170 GeV, Fig. 14. Below this energy it increses significantly for the reasons discussed above; above 170 GeV there is a very slight increase from phase space effects. Coulomb effects narrow the mass distribution at around threshold, Fig. 15. Again this behaviour can be related to the width of the momentum distribution, Fig. 16, and to a narrowing of the width when Coulomb effects are included, Fig. 17. In general, however, the relation between $\sigma_m - \sigma_{m,\mathrm{nC}}$ and $\sigma_p - \sigma_{p,\mathrm{nC}}$ is not as straightforward as between $\langle m \rangle - \langle m_{\mathrm{nC}} \rangle$ and $\langle p \rangle - \langle p_{\mathrm{nC}} \rangle$. This is because the factor p in the $\delta m \approx -p\delta p/m$ relation suppresses the importance of the low-momentum tail on the mass distribution, while it enhances the importance of the high-momentum tail. Thus the stable-Coulomb scenario has a broader momentum distribution than the no-Coulomb one at most energies, but since this is due mainly to the enhancement of the low-momentum tail, the mass distribution may still be narrower. In the unstable-Coulomb approaches, the enhancement is in the high-momentum tail, and thus the momentum and mass width changes better follow suit.

As we have noted earlier, experimental W mass methods are based on the p observable rather than on the m_1 and m_2 ones. That is, measured jet/lepton directions and energies are not used to reconstruct two masses per event. Instead the two W's are assumed

to have the same mass, and beam energy constraints are used to improve the detector energy resolution, so that most of the experimental information is related to angles and from there to the net momentum of jet pairs, i.e. to p. The translation from a set of p measurements to a W mass can be done in different ways, that are more or less sensitive to Coulomb effects. Compare Figs. 18 and 19; in the former the momentum p is first averaged over events and then translated to an average mass, $\langle m \rangle = \sqrt{s/4 - \langle p \rangle^2}$, in the latter the p's are first translated to m's and then averaged, $\langle m \rangle = \langle \sqrt{s/4 - p^2} \rangle$. It turns out that the former recipe is preferrable in the threshold region, in that it gives a smaller spread between the alternatives, while there is no noticeable difference at higher energies.

Other averaging schemes can be considered, where also events are giving relative weights to reflect their "usefulness" in constraining the W mass. The most direct approach is to remove some fraction of the events in the wings of the momentum distributions, where events are found only if one of the W's is significantly off the mass shell. For experimental rejection of background events, such an approach offers additional benefits. The importance of the wings for the momentum shift of Coulomb effects is shown in Fig. 20 for a few energies. What is plotted is

$$\frac{\mathrm{d}\Delta\langle p \rangle}{\mathrm{d}p} = \frac{\mathrm{d}(\langle p_{\mathrm{C}} \rangle - \langle p_{\mathrm{nC}} \rangle)}{\mathrm{d}p} = (p - \langle p \rangle_{\mathrm{nC}}) \left(\frac{1}{\sigma_{\mathrm{C}}} \frac{\mathrm{d}\sigma_{\mathrm{C}}}{\mathrm{d}p} - \frac{1}{\sigma_{\mathrm{nC}}} \frac{\mathrm{d}\sigma_{\mathrm{nC}}}{\mathrm{d}p} \right) , \qquad (17)$$

where index "C" ("nC") denotes a scenario with (without) Coulomb effects. By construction, the measure vanishes at $\langle p \rangle_{\mathrm{nC}}$; this is visible at the lower energies but is somewhat hidden by the finite resolution at the highest energies. In other words, the shift of the average momentum is dominated by the behaviour in the wings at low energies. At higher energies, the momentum distribution is narrower and also the shift of the average momentum is dominated by a smaller region. This behaviour carries over to the mass shift $\langle m \rangle - \langle m_{\mathrm{nC}} \rangle$. We study two alternatives, keeping only those events with momentum within 30 and 10 GeV, respectively, of the average. For simplicity, $\langle p \rangle$ has here been approximated by the expression $\langle p \rangle_{\mathrm{approx}} = \sqrt[4]{(s/4 - M_{\mathrm{W}}^2)^2 + 4M_{\mathrm{W}}^2\Gamma_{\mathrm{W}}^2}$, which is not particularly accurate below threshold but good enough for this purpose. Comparing the mass shifts in Figs. 21 and 22 with those in Fig. 9, we note the reduced importance of Coulomb effects below and around threshold, while the reduction is rather modest at higher energies. For instance, at a typical LEP 2 energy of 175 GeV, the difference between unstable Coulomb and no Coulomb decreases from -23 MeV without cut to -16 MeV with a cut $|p - \langle p \rangle_{\mathrm{approx}}| < 10$ GeV. The statistics will drop if the momentum window is reduced further, so it appears difficult to do much better.

We have compared several alternative Coulomb effect scenarios in this paper. Thereby we hope to learn about the possible effects also of other (not yet calculated) QED effects, like intermediate–final interference. Whereas a scenario such as the no-Coulomb one obviously is excluded, we have above indicated how something akin to it might arise as an approximate description of the normalized momentum distribution. Such ambiguities would be resolved if the experimental data themselves could be used to extract the form of QED corrections. One specific idea would be to divide the experimental momentum spectrum by the no-Coulomb rate, to obtain a distribution akin to what is shown in Fig. 4. If the experimental distribution would agree with contemporaneous calculations, theory could be used to extract the W mass. If not, the experimentally defined correction factors could still be used for this purpose.

There are two major problems with such a thinking, however. Firstly, so long as we

do not know the W mass we also do not know which no-Coulomb curve to compare with. The sharp increase in the unstable Coulomb factor at around p_0 for the higher energies in Fig. 4 is there since we compare scenarios with the same M_{W}. If instead $\langle p \rangle$ is made to agree, as would be the realistic experimental procedure, differences between scenarios are not as spectacular. Still, even with the same $\langle p \rangle$, the shape of the momentum spectrum would be different, so with hard work it should be possible to find which descriptions work and which do not. However, here enters the second problem, namely that of limited statistics. A LEP 2 experiment will at most have of order 10,000 events to base the analysis on. It is difficult to see how this would be enough to observe any differences, given that we are speaking of Coulomb correction factors of a few per cent.

This prejudice is borne out by detailed studies. For instance, in Fig. 23 we have compared 100 "LEP 2 experiments" at 175 GeV, each of 10000 events. In the stable-Coulomb scenario the M_{W} parameter has been shifted down by 13 MeV relative to the no-Coulomb one, and in the unstable-Coulomb one up by 22 MeV (cf. Fig. 9), so that $\langle p \rangle$ should be the same. In fact, the limited statistics leads to a non-negligible spread of $\langle p \rangle$ values. Also higher moments, in Fig. 23 $\sqrt[n]{\langle (p - \langle p \rangle)^n \rangle}, n = 2, 3, 4$, show a significant statistical spread, with no obvious separation between the no-, stable- and unstable-Coulomb scenarios. For a given "LEP 2 experiments" it is impossible to tell which distribution it is drawn from. Correlations between the moments again do not distinguish (not shown).

One therefore must conclude that — unless something truly spectacular happens — experimental input can not be used to pin down QED interconnection effects. It is necessary to have the theory under control to the required accuracy.

4 Conclusions

One of the most critical single observables for LEP 2 physics is the W mass. Had there been no interconnection effects between the W^+ and the W^-, in principle their respective four-momenta could be reconstructed and squared to give the $\mathrm{W}^\pm$ masses. The shifts in the observable W mass distributions could come from a number of sources [8, 9, 10] that we have not attempted to address here. Our main concern has been to estimate the W mass shift caused by distortions of the W momentum spectrum from instability effects, as embodied in the QED radiative corrections to the differential $\mathrm{e}^+\mathrm{e}^- \to \mathrm{W}^+\mathrm{W}^-$ cross section. In the threshold region we can exploit the formulae for Coulomb corrections [2, 14], which here are responsible for the dominant off-shellness-induced phenomena. For complete predictions in the whole LEP 2 energy range, one needs to incorporate the contributions of other QED interconnection mechanisms, e.g. those resulting from intermediate–final and final–final photon interference [3, 13]. As far as we are aware, the complete analytical calculation has never been performed for the whole set of electroweak corrections to unstable W production and decay. (An attempt to estimate QED interconnection phenomena in the relativistic region can be found in ref. [13].)

While the complete calculation is missing, one may attempt to compare some different scenarios that give an impression of the size of effects. Our current "best" description is the all-orders Coulomb description in ref. [21]. One conclusion of this paper is that second-order (and, by implication, all higher-order) Coulomb effects are practically negligible. The first-order ("unstable") Coulomb description therefore is a realistic baseline. Other intermediate–final and final–final interference terms are expected to modify this behaviour. Specifically, one could expect the rapid variation of the Coulomb factor around

p_0 (the on-mass-shell W momentum) to be substantially dampened. In fact, a brute-force application of a proposed asymptotic dampening factor [13] to the LEP 2 energy region would imply that a momentum-dependent Coulomb factor can be replaced by an almost momentum-independent average. Therefore the no-Coulomb scenario could be a realistic alternative for reconnection effects on kinematical distributions. The final scenario, with Coulomb effects evaluated for stable W's, is less realistic and has been included mainly for completeness.

At LEP 2 energies, the no- and unstable-Coulomb scenarios differ by about 20 MeV on the observable $\langle m \rangle$, given a common theory input M_{W}. This is somewhat below the statistical accuracy, but comparable with other potential sources of systematic error, and so not negligible. It is therefore interesting to see whether the uncertainty can be reduced by a clever choice of experimental procedure. The conclusions of this paper are not too optimistic on this count. The limited statistics will preclude the testing of the theory scenarios from data itself. One will therefore be totally dependent on a full-scale theory calculation to reach any definite conclusions. However, different statistical treatments of the data can increase or decrease the 20 MeV number above by some amount: in the paper we have given the examples of cuts on the momentum range analyzed and choice of statistical averaging procedure.

The QED final-state interaction could induce some systematic effects in other W-mass measurements as well, for instance in $\overline{\mathrm{p}}\mathrm{p}$ collider experiments. Of particular interest here is the subprocess $\mathrm{qg} \to \mathrm{Wq}'$ with $\mathrm{W} \to \ell\nu_\ell$. Collider experiments normally rely on the equivalent process for Z^0 production, $\mathrm{qg} \to \mathrm{Zq}$ with $\mathrm{Z} \to \ell^+\ell^-$, to calibrate the W mass scale. Non-universal interference effects are not included in such a procedure, e.g. a charged ($\mathrm{W}^\pm$) versus a chargeless (Z^0) intermediate state. The effects of real-photon emission have been compared [22], but virtual corrections remain to be studied. It could well turn out that a corresponding theory uncertainty of order 20 MeV exists in this process. Within current experimental errors this would be negligible, but it could become relevant for future high-precision measurements.

Acknowledgements

We are grateful to the UK PPARC for support. Useful discussions with V.S. Fadin, N. Kjaer, K. Melnikov, R. Møller, W.J. Stirling and O. Yakovlev are acknowledged. This work was supported in part by the EU Programme "Human Capital and Mobility", Network "Physics at High Energy Colliders", contract CHRX-CT93-0319 (DG 12 COMA).

References

[1] W.J. Stirling, University of Durham preprint DTP/95/24 (1995)

[2] V.S. Fadin, V.A. Khoze and A.D. Martin, Phys. Lett. **B311** (1993) 311

[3] V.S. Fadin, V.A. Khoze and A.D. Martin, Phys. Rev. **D49** (1994) 2247; Phys. Lett. **B320** (1994) 141

[4] K. Melnikov and O. Yakovlev, Phys. Lett. **B324** (1994) 217

[5] Y. Sumino, Univ. of Tokyo preprint UT-655 (1993)

[6] For reviews on $t\bar{t}$ threshold physics see, e.g.,
J.H. Kühn, Proc. Workshop on Physics and Experiments with Linear e^+e^- Colliders, eds. F.A. Harris et al. (World Scientific, Singapore, 1993), p. 72;
Y. Sumino, Acta Phys. Polon. **B25** (1994) 1837

[7] V.S. Fadin and V.A. Khoze, Proc. 24th LNPI Winter School, Vol. I, p. 3, Leningrad (1989)

[8] T. Sjöstrand and V.A. Khoze, Phys. Rev. Lett. **72** (1994) 28; Z. Phys. **C62** (1994) 281

[9] J. Bijnens et al., *Measurement of the W mass at LEP 200*, in ECFA Report on LEP 200, eds. A. Böhm and W. Hoogland, CERN-87-08 and ECFA 87/108 (1987), Vol. I, p. 49;
S. Katsanevas et al., *Report from the Working Group on LEP 200 Physics*, DELPHI 92-166 PHYS250 (1992);
various presentations in the W mass group of the LEP 2 physics workshop (1995)

[10] L. Lönnblad and T. Sjöstrand, Phys. Lett. **B351** (1995) 293

[11] J.H. Bijnens and R. Møller, private communication

[12] For a recent review and further references see, e.g.,
W. Beenakker and A. Denner, Int. J. Mod. Phys **A9** (1994) 4837

[13] K. Melnikov and O. Yakovlev, University of Mainz preprint MZ-TH/95-01 (1995), to be published in Nucl. Phys **B**

[14] V.S. Fadin, V.A. Khoze, A.D. Martin and A. Chapovsky, Phys. Rev. **D52** (1995) 1377

[15] D. Bardin, W. Beenakker and A. Denner, Phys. Lett. **B317** (1993) 213

[16] V.A. Khoze and W.J. Stirling, University of Durham preprint DTP/95/42 (1995), to be published in Phys. Lett. **B**

[17] V.S. Fadin and V.A. Khoze, JETP Lett. **46** (1987) 525; Sov. J. Nucl. Phys. **48** (1988) 309; **53** (1991) 692

[18] A. Sommerfeld, *Atombau und Spektrallinien*, Bd. 2, Vieweg, Braunschweig (1939); A.D. Sakharov, JETP **18** (1948) 631.

[19] CDF collaboration, F. Abe et al., Phys. Rev. Lett. **75** (1995) 11, preprint FERMILAB-PUB-95/033-E (1995)

[20] T. Muta, R. Najima and S. Wakaizumi, Mod. Phys. Lett. **A1** (1986) 203.

[21] V.S. Fadin, V.A. Khoze, A.D. Martin and W.J. Stirling, University of Durham preprint DTP/95/64 (1995)

[22] U. Baur and D. Zeppenfeld, preprint MAD/PH/878 and UB–HET–95-02

Figure Captions

Fig. 1 Total $e^+e^- \to W^+W^-$ cross section σ as a function of the c.m. energy. Dashed-dotted curve is no Coulomb, dashed stable Coulomb, full unstable Coulomb and dotted second-order Coulomb.

Fig. 2 Total cross section relative to the no-Coulomb one, σ/σ_0. Notation as in Fig. 1.

Fig. 3 The differential cross section $\mathrm{d}\sigma/\mathrm{d}p$ in pb/GeV. Notation as in Fig. 1.

Fig. 4 Ratio of the differential cross sections with and without Coulomb effects included, $(\mathrm{d}\sigma/\mathrm{d}p)_{\mathrm{C}}/(\mathrm{d}\sigma/\mathrm{d}p)_{\mathrm{nC}}$. Dashed curve is stable Coulomb, full unstable Coulomb and dotted second-order Coulomb. At the two highest energies, dashed-dotted curve is dampened Coulomb.

Fig. 5 Ratio of second- to first-order Coulomb corrections, $(|f(\mathbf{p},E)|^2 - 1 - \alpha\overline{\delta}_{\mathrm{C}}/\beta)/(\alpha\overline{\delta}_{\mathrm{C}}/\beta)$, as a function of p. The dashed line at small p indicates the $p \to 0$ limit given in eq. (16).

Fig. 6 Average W momentum, $\langle p \rangle$. Notation as in Fig. 1.

Fig. 7 Shift of the average W momentum relative to the no-Coulomb value, $\langle p \rangle - \langle p_{\mathrm{nC}} \rangle$. Notation as in Fig. 1.

Fig. 8 Shift of the average W mass relative to the nominal one, $\langle m \rangle - M_{\mathrm{W}}$. Notation as in Fig. 1.

Fig. 9 Shift of the average W mass relative to the no-Coulomb value, $\langle m \rangle - \langle m_{\mathrm{nC}} \rangle$. Notation as in Fig. 1.

Fig. 10 Shift of the lighter W mass relative to the no-Coulomb value, $(\langle m \rangle - \langle m_{\mathrm{nC}} \rangle)_{\mathrm{light}}$. Notation as in Fig. 1.

Fig. 11 Shift of the heavier W mass relative to the no-Coulomb value, $(\langle m \rangle - \langle m_{\mathrm{nC}} \rangle)_{\mathrm{heavy}}$. Notation as in Fig. 1.

Fig. 12 Root-mean-square width of the lighter W mass distribution, $\sigma_{m,\mathrm{light}}$. Notation as in Fig. 1.

Fig. 13 Root-mean-square width of the heavier W mass distribution, $\sigma_{m,\mathrm{heavy}}$. Notation as in Fig. 1.

Fig. 14 Root-mean-square width of the average W mass distribution, σ_m. Notation as in Fig. 1.

Fig. 15 Shift of the width of the average W mass distribution relative to the no-Coulomb value $\sigma_m - \sigma_{m,\mathrm{nC}}$. Notation as in Fig. 1.

Fig. 16 Root-mean-square width of the W momentum distribution, σ_p. Notation as in Fig. 1.

Fig. 17 Shift of the width of the W momentum distribution relative to the no-Coulomb value, $\sigma_p - \sigma_{p,\mathrm{nC}}$. Notation as in Fig. 1.

Fig. 18 Shift of the average W mass relative to the no-Coulomb value, $\langle m \rangle - \langle m_{\mathrm{nC}} \rangle$. Here the average momentum $\langle p \rangle$ has been converted into an average mass $\langle m \rangle = \sqrt{s/4 - \langle p \rangle^2}$. Notation as in Fig. 1.

Fig. 19 Shift of the average W mass relative to the no-Coulomb value, $\langle m \rangle - \langle m_{\mathrm{nC}} \rangle$. Here the momentum p in each event has been converted into an effective mass $m = \sqrt{s/4 - p^2}$, and this mass has been averaged over events. Notation as in Fig. 1.

Fig. 20 The buildup of the total shift in $\langle p \rangle$ as a function of p, as given in eq. (17). The result is given in relation to the no-Coulomb alternative. Dashed curve is stable Coulomb, full unstable Coulomb and dotted second-order Coulomb.

Fig. 21 Shift of the average W mass relative to the no-Coulomb value, $\langle m \rangle - \langle m_{\mathrm{nC}} \rangle$. Here only events with $|p - \langle p \rangle_{\mathrm{approx}}| < 30$ GeV have been included. Notation as in Fig. 1.

Fig. 22 Shift of the average W mass relative to the no-Coulomb value, $\langle m \rangle - \langle m_{\mathrm{nC}} \rangle$. Here only events with $|p - \langle p \rangle_{\mathrm{approx}}| < 10$ GeV have been included. Notation as in Fig. 1.

Fig. 23 The distribution of some moments of the momentum distribution in 100 "LEP 2 experiments" of 10000 events each at 175 GeV. Dashed-dotted histogram is no Coulomb, dashed stable Coulomb, and full unstable Coulomb. The M_{W} mass parameter has been adjusted to give the same $\langle p \rangle$ in the three scenarios.

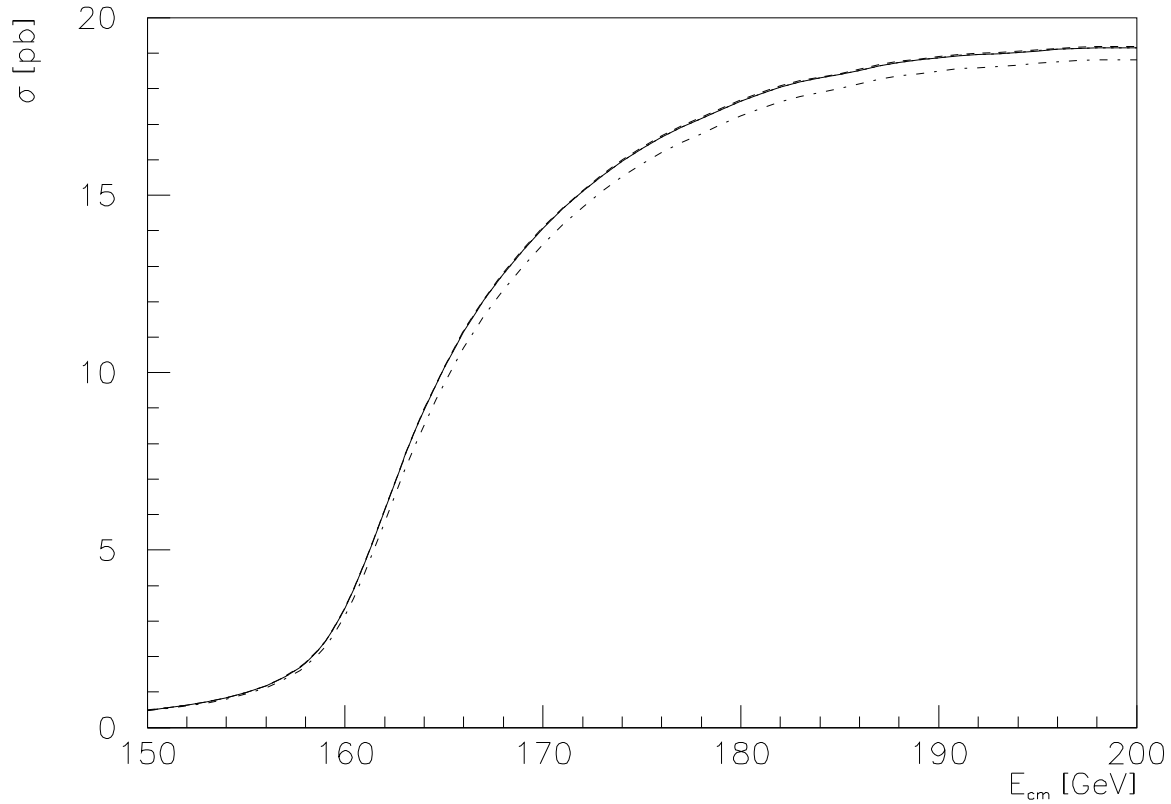

Figure 1

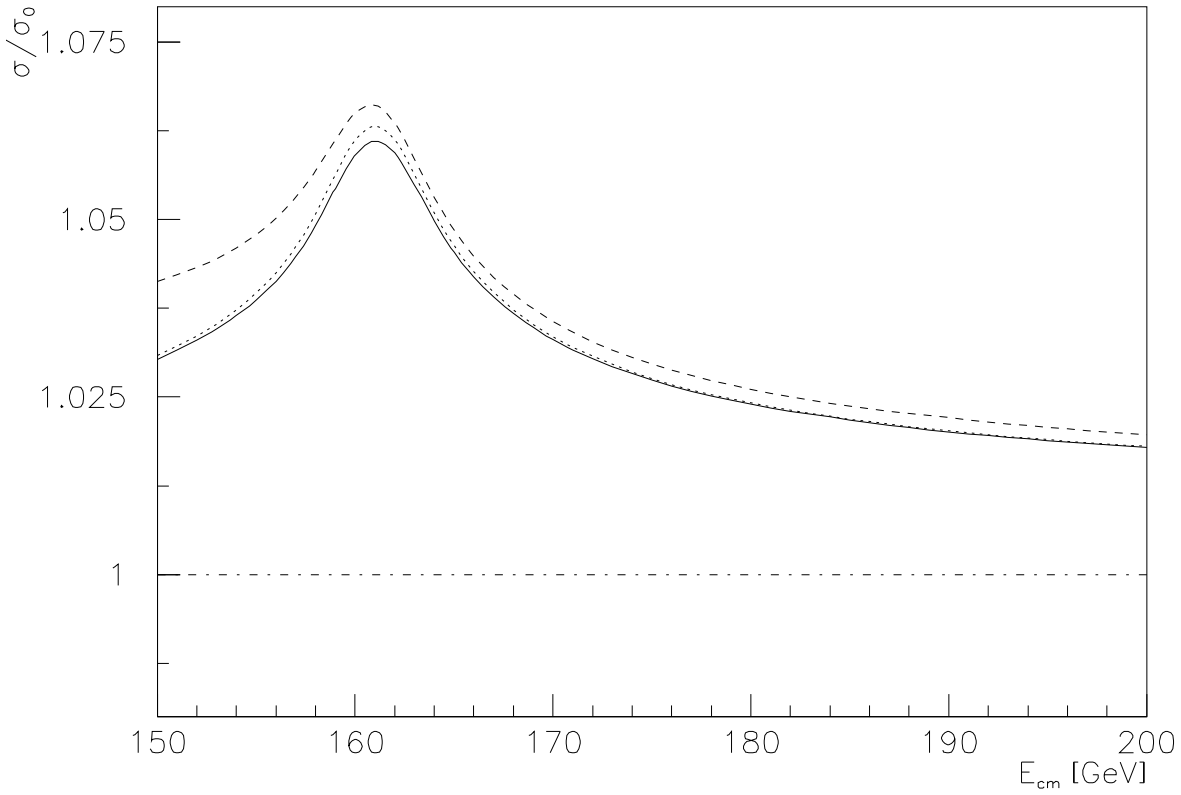

Figure 2

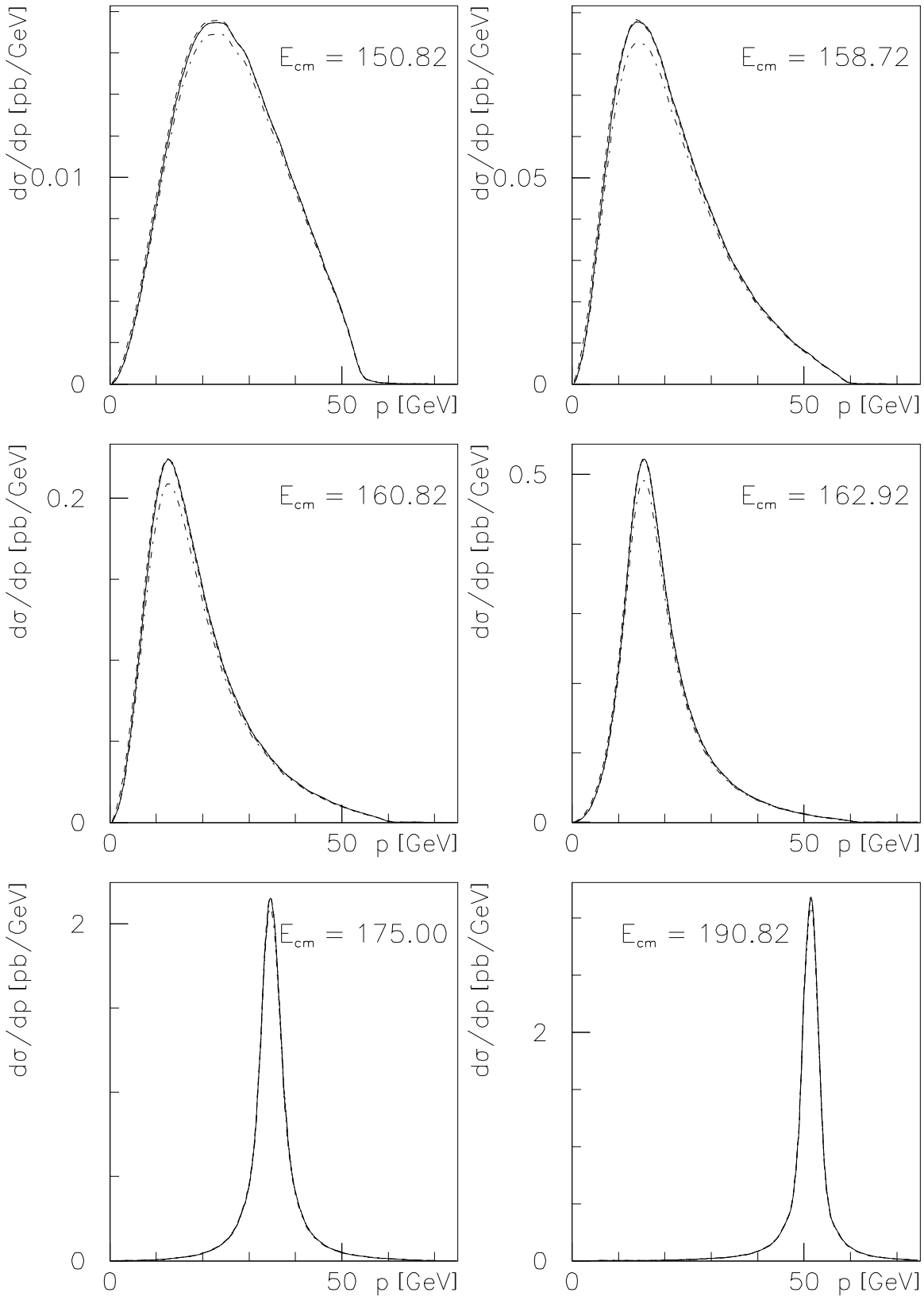
dσ/dp [pb/GeV]
0.01
0
0
50 p [GeV]
E_cm = 150.82
dσ/dp [pb/GeV]
0.05
0
0
50 p [GeV]
E_cm = 158.72
dσ/dp [pb/GeV]
0.2
0
0
50 p [GeV]
E_cm = 160.82
dσ/dp [pb/GeV]
0.5
0
0
50 p [GeV]
E_cm = 162.92
dσ/dp [pb/GeV]
2
0
0
50 p [GeV]
E_cm = 175.00
dσ/dp [pb/GeV]
2
0
0
50 p [GeV]
E_cm = 190.82

Figure 3

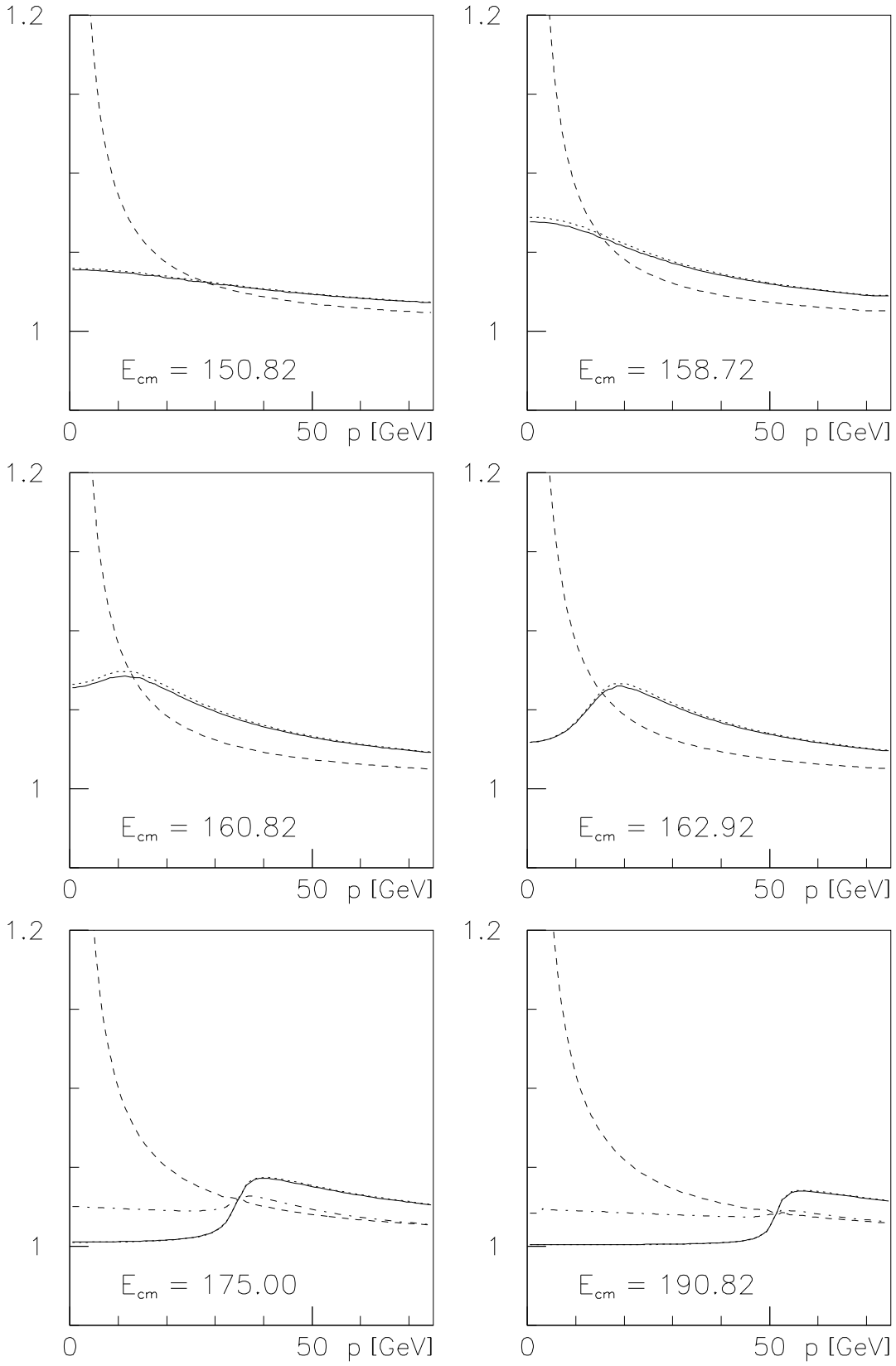
1.2
1
0
50 p [GeV]
E_{cm} = 150.82
E_{cm} = 158.72
E_{cm} = 160.82
E_{cm} = 162.92
E_{cm} = 175.00
E_{cm} = 190.82

Figure 4

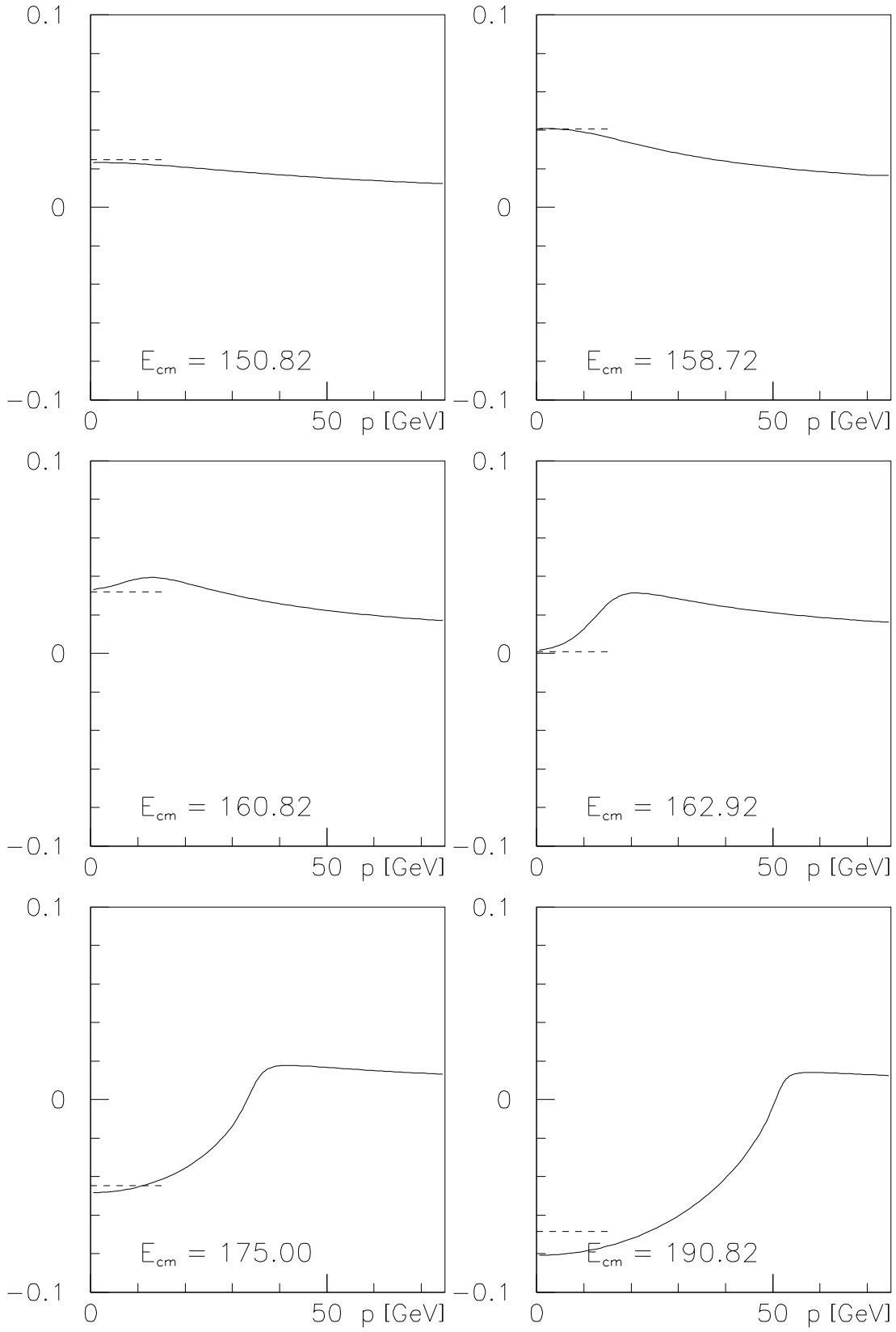
0.1
0
−0.1
0
50 p [GeV]
E_{cm} = 150.82
E_{cm} = 158.72
E_{cm} = 160.82
E_{cm} = 162.92
E_{cm} = 175.00
E_{cm} = 190.82

Figure 5

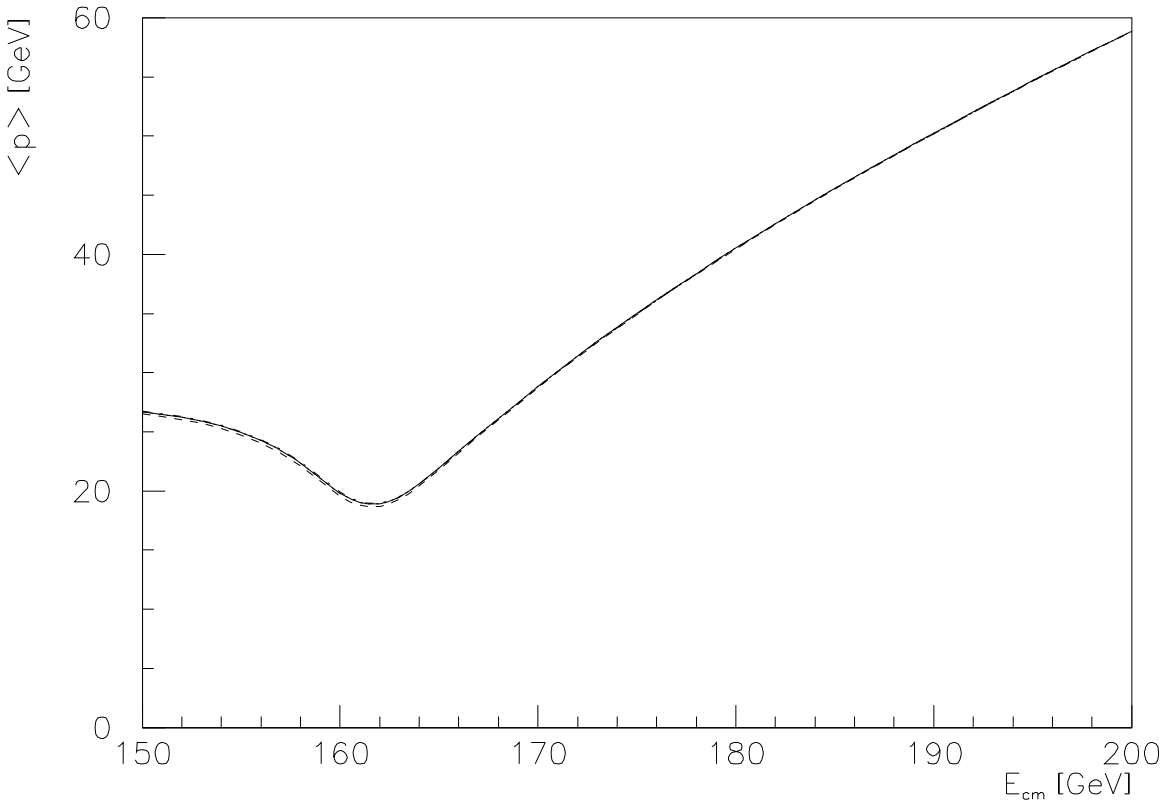

Figure 6

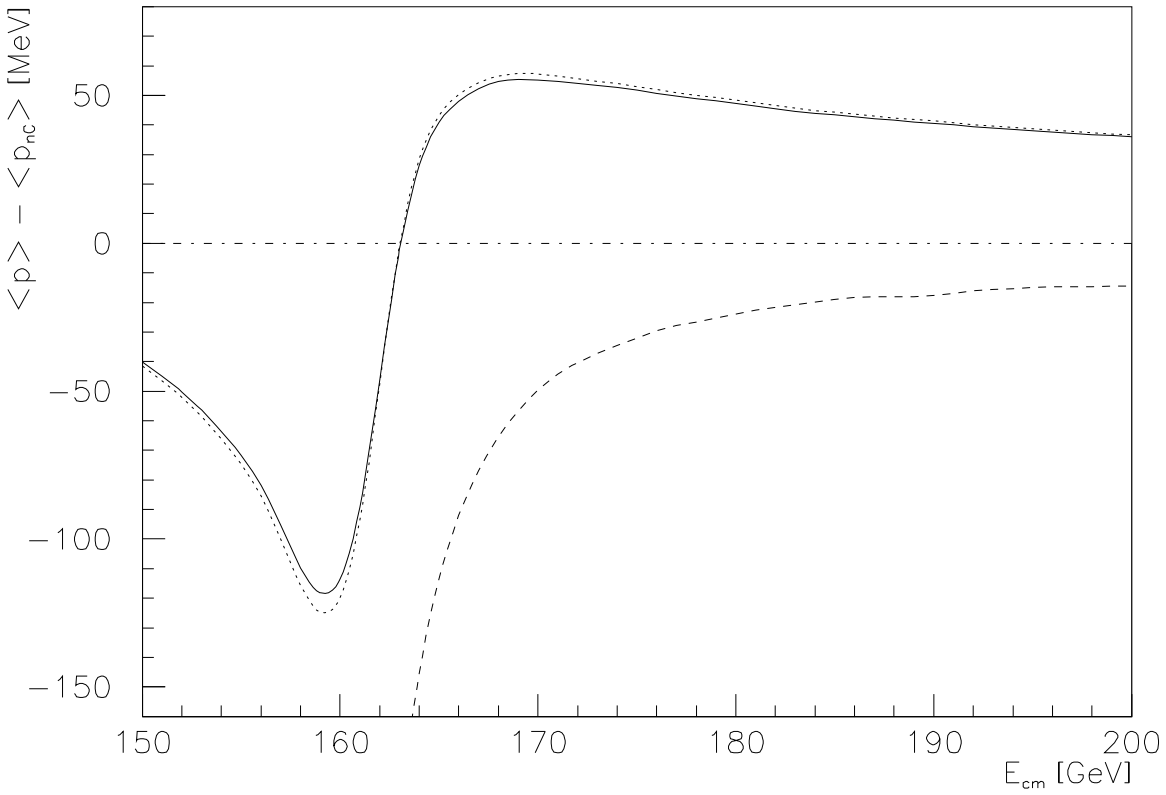

Figure 7

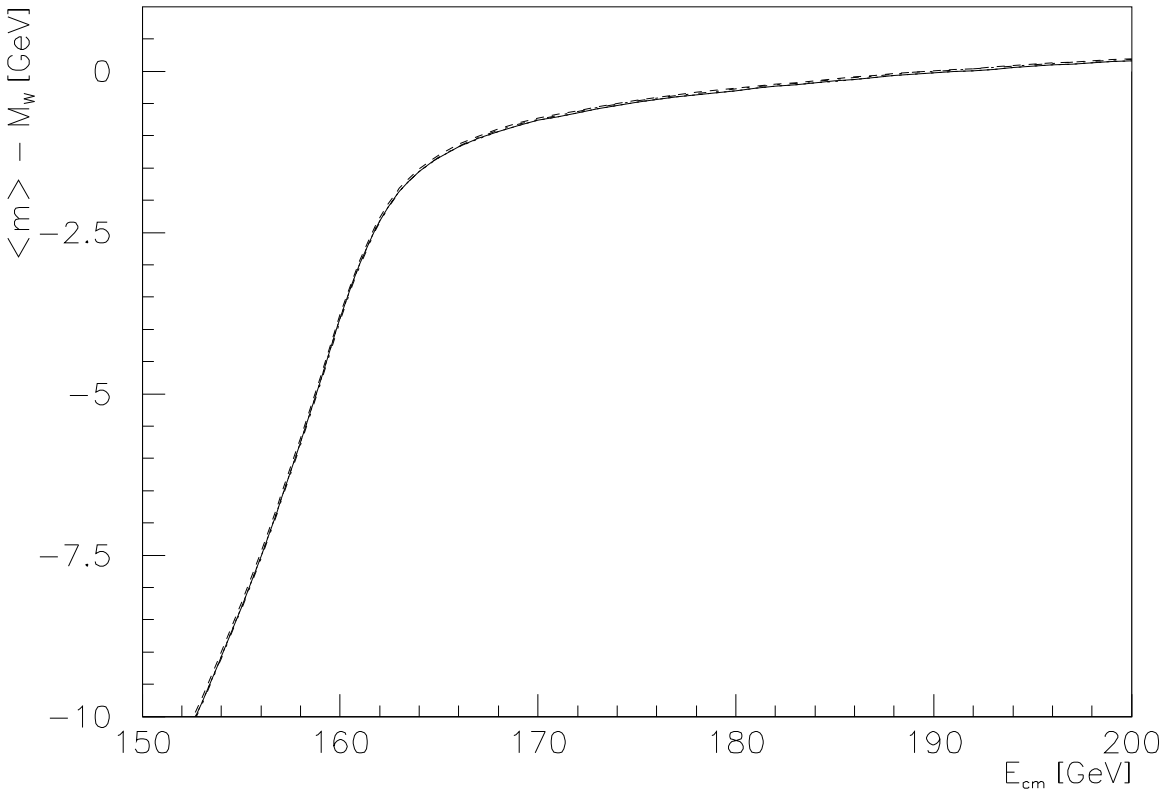

Figure 8

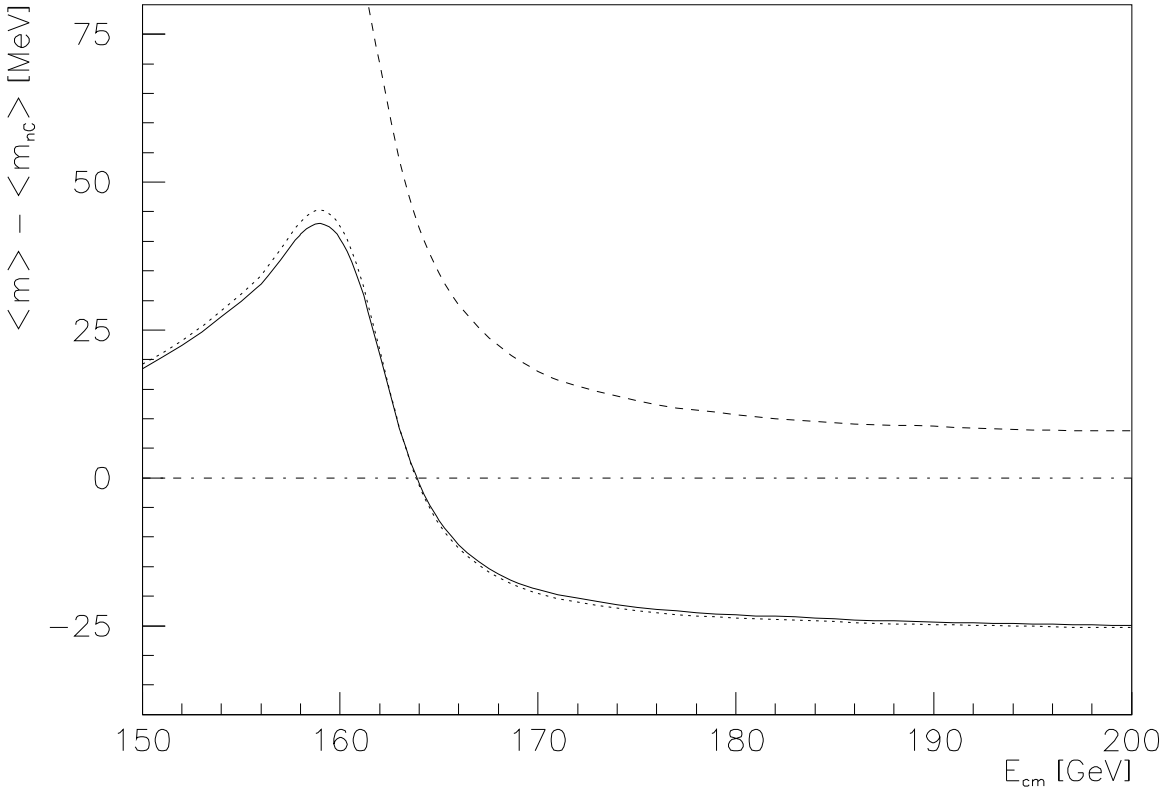

Figure 9

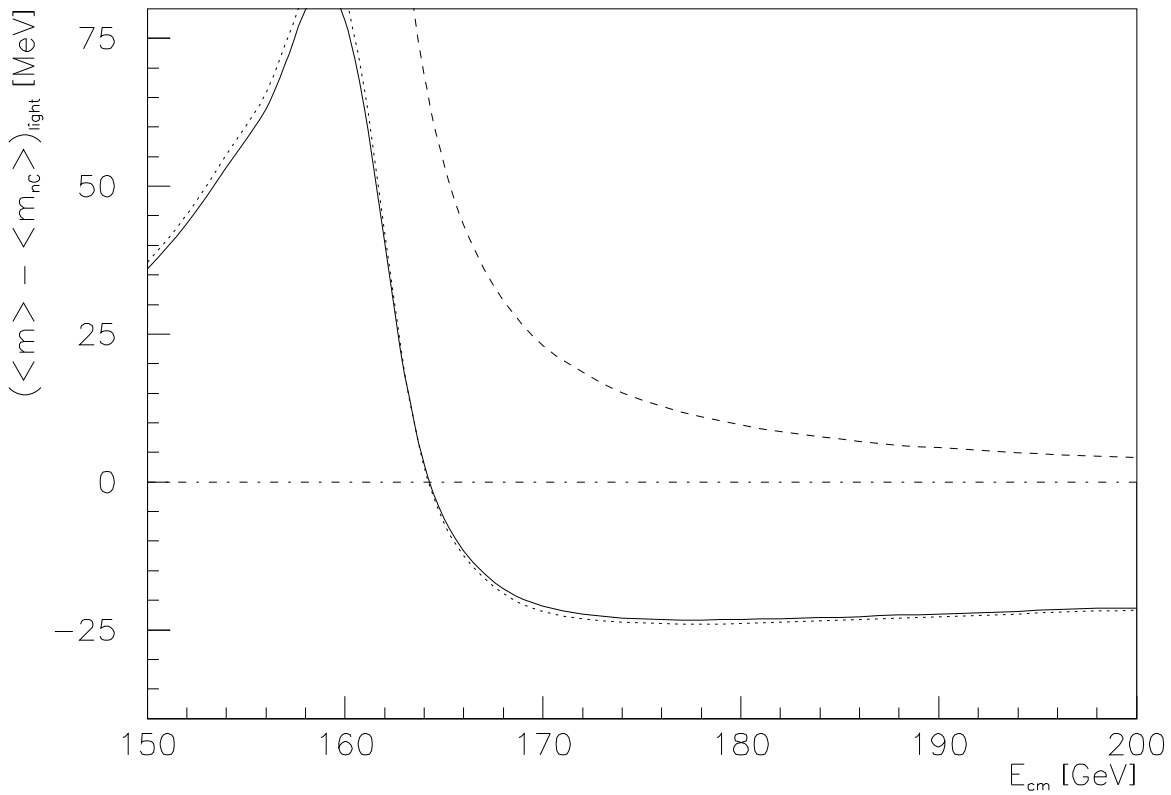

Figure 10

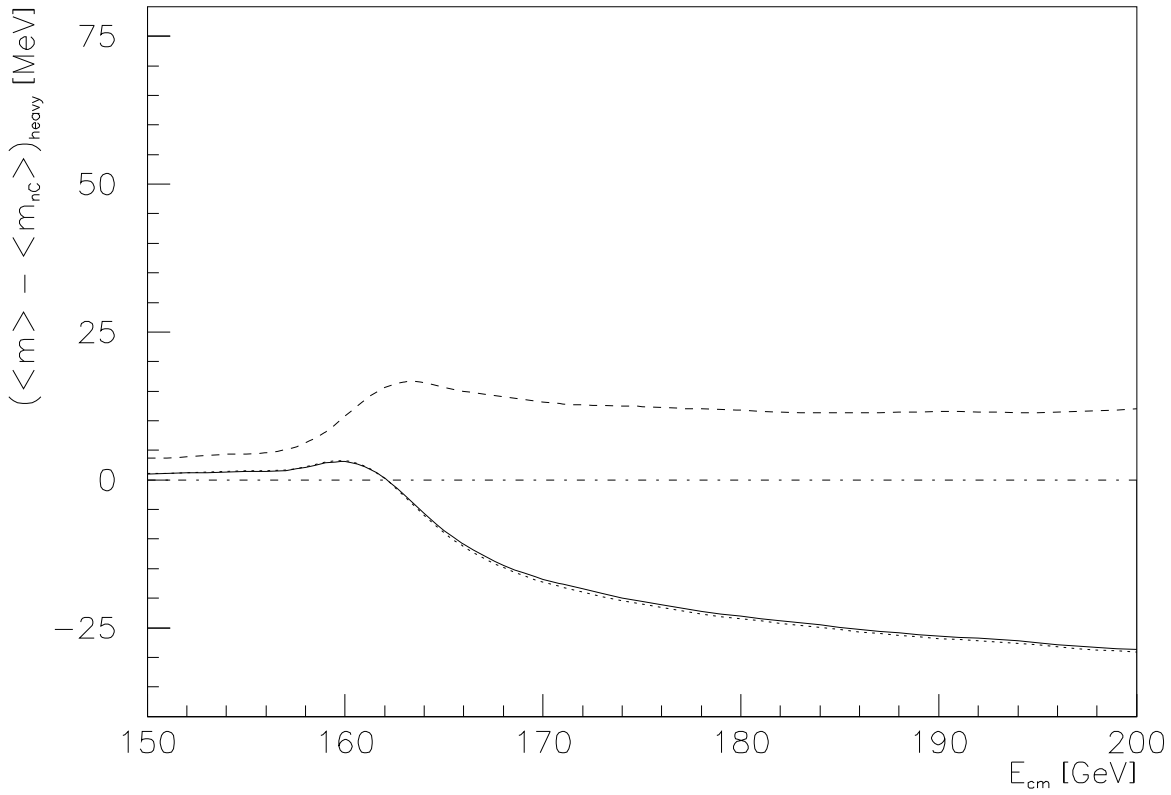

Figure 11

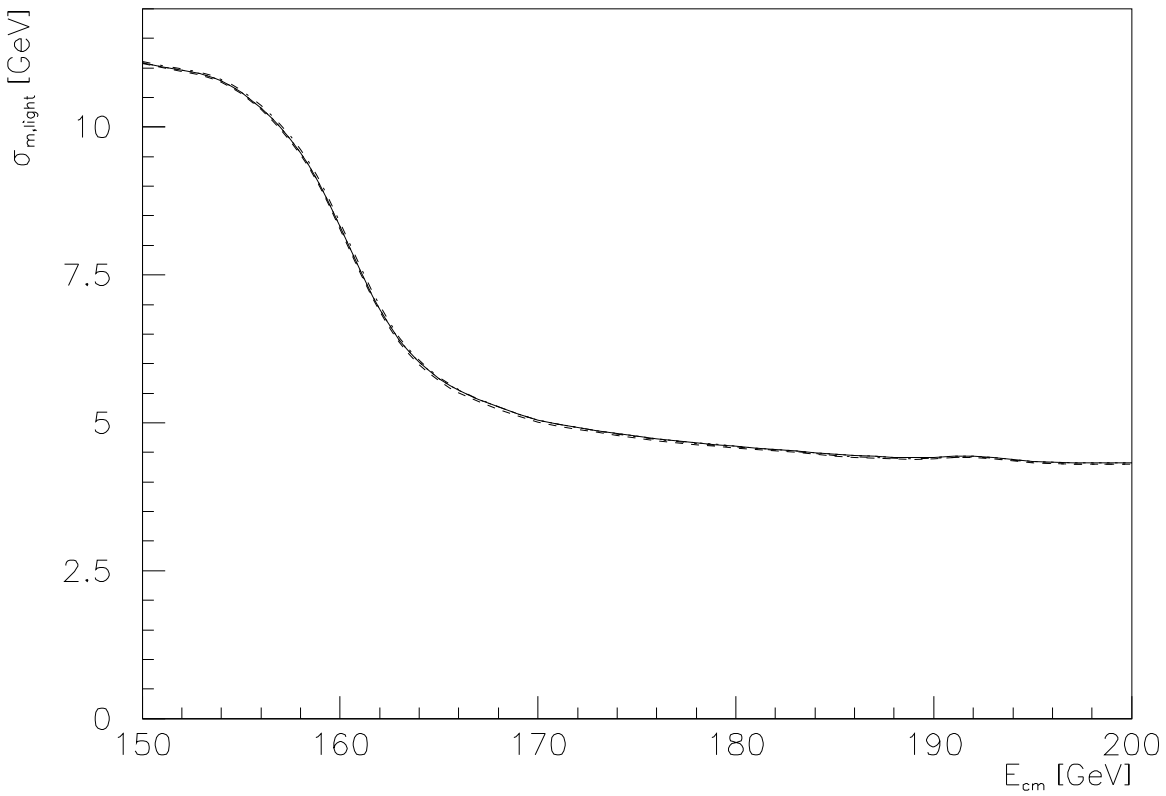

Figure 12

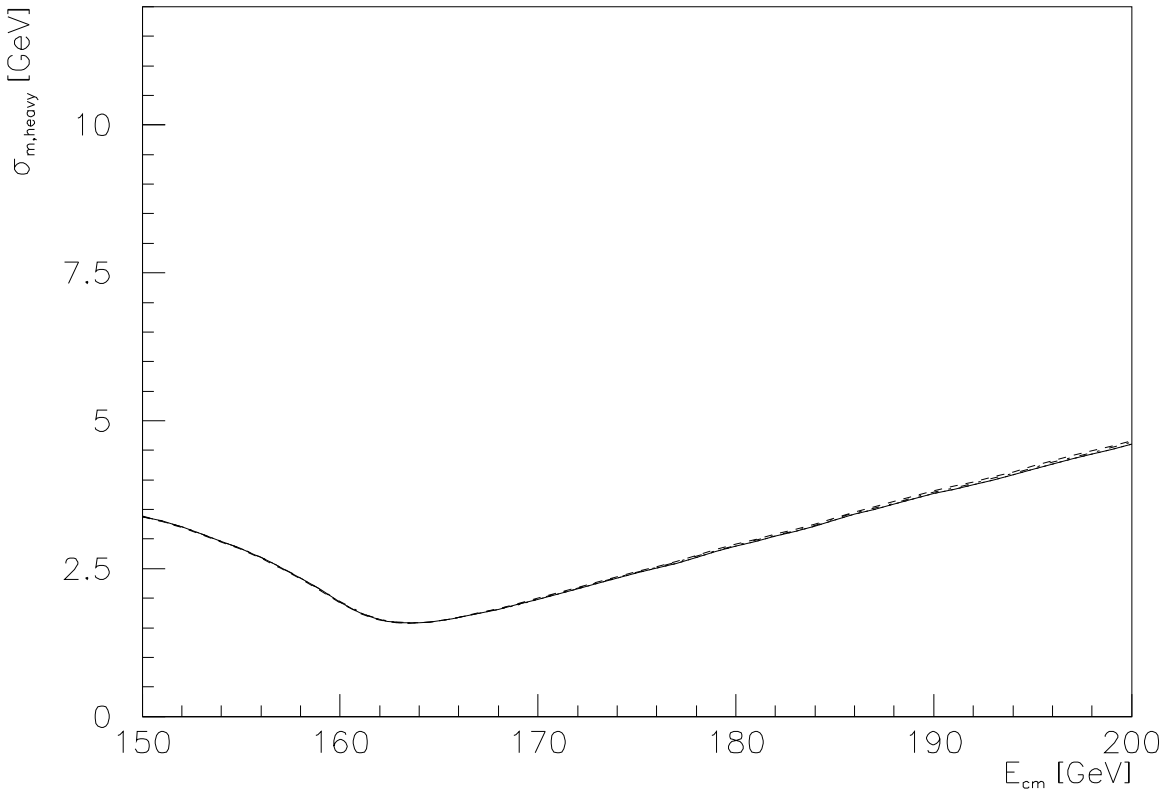

Figure 13

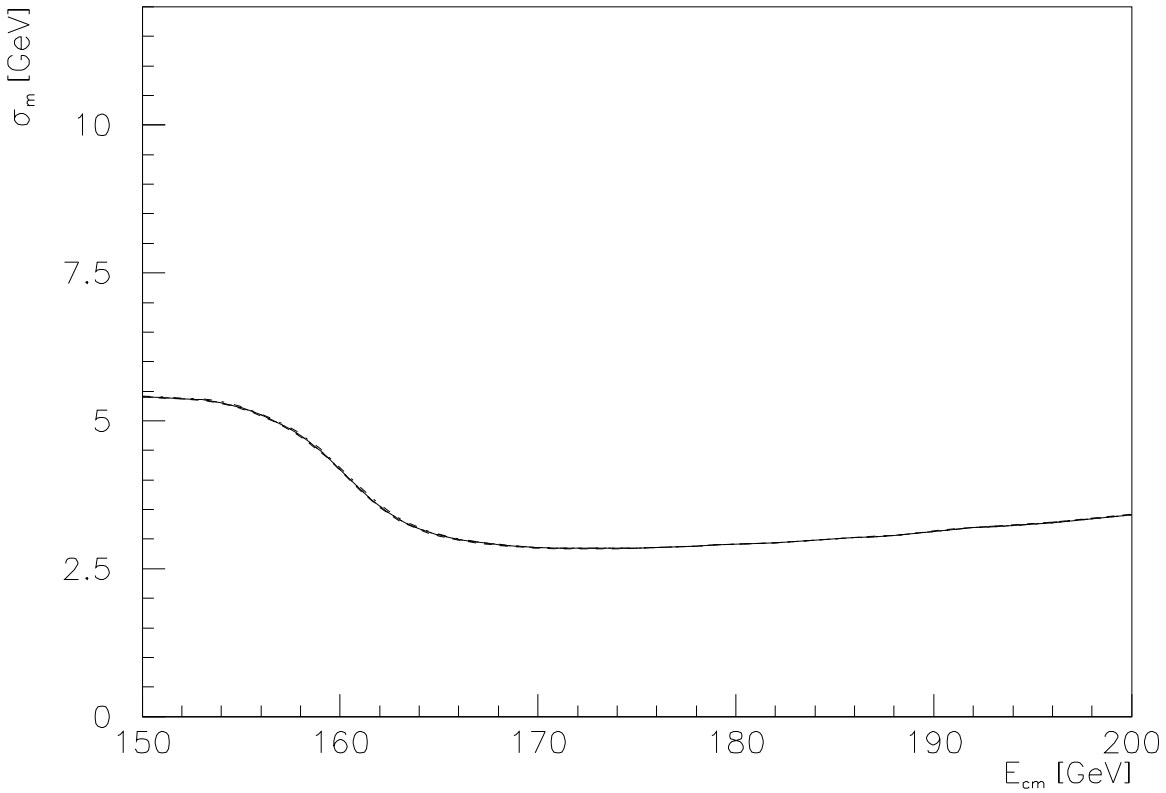

Figure 14

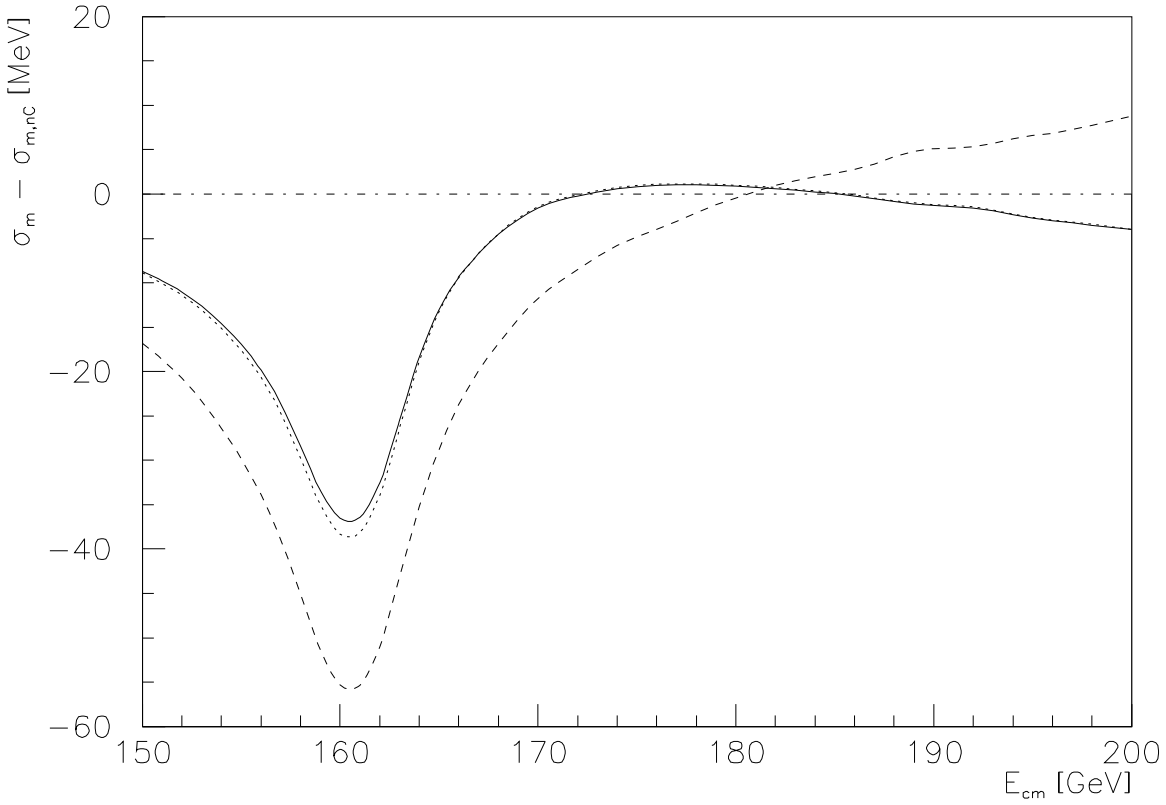

Figure 15

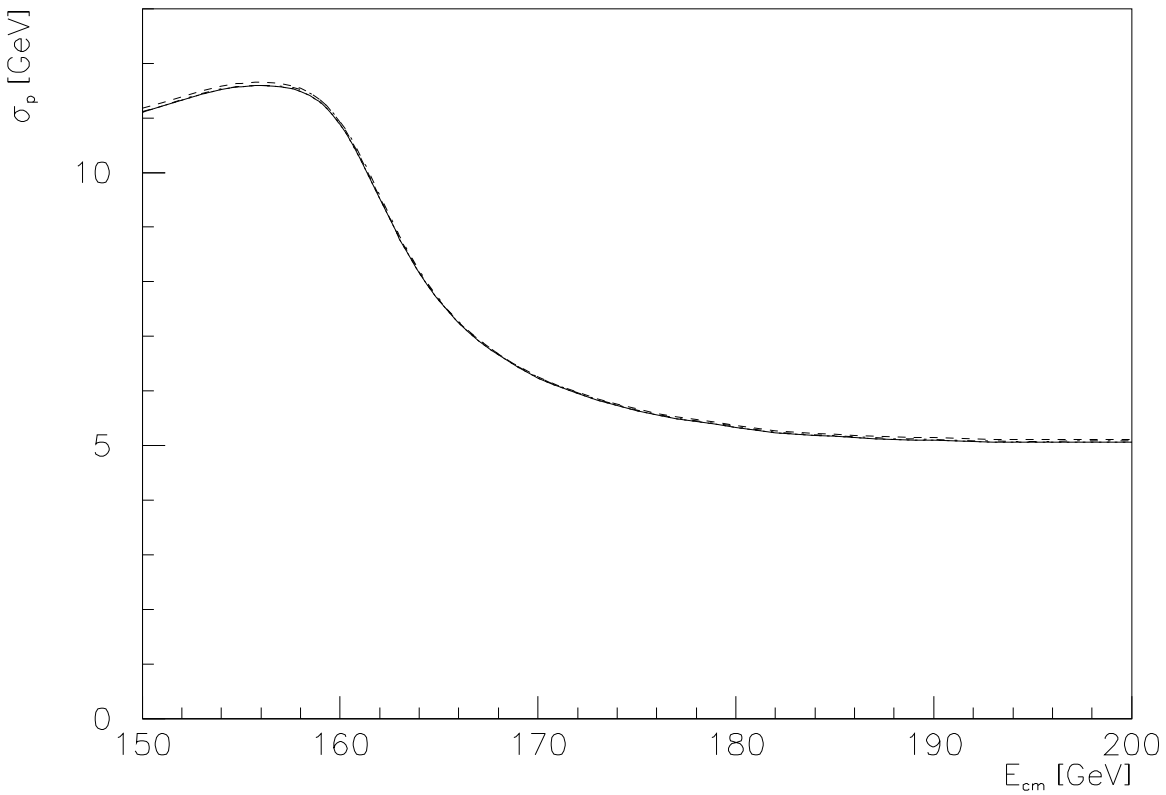

Figure 16

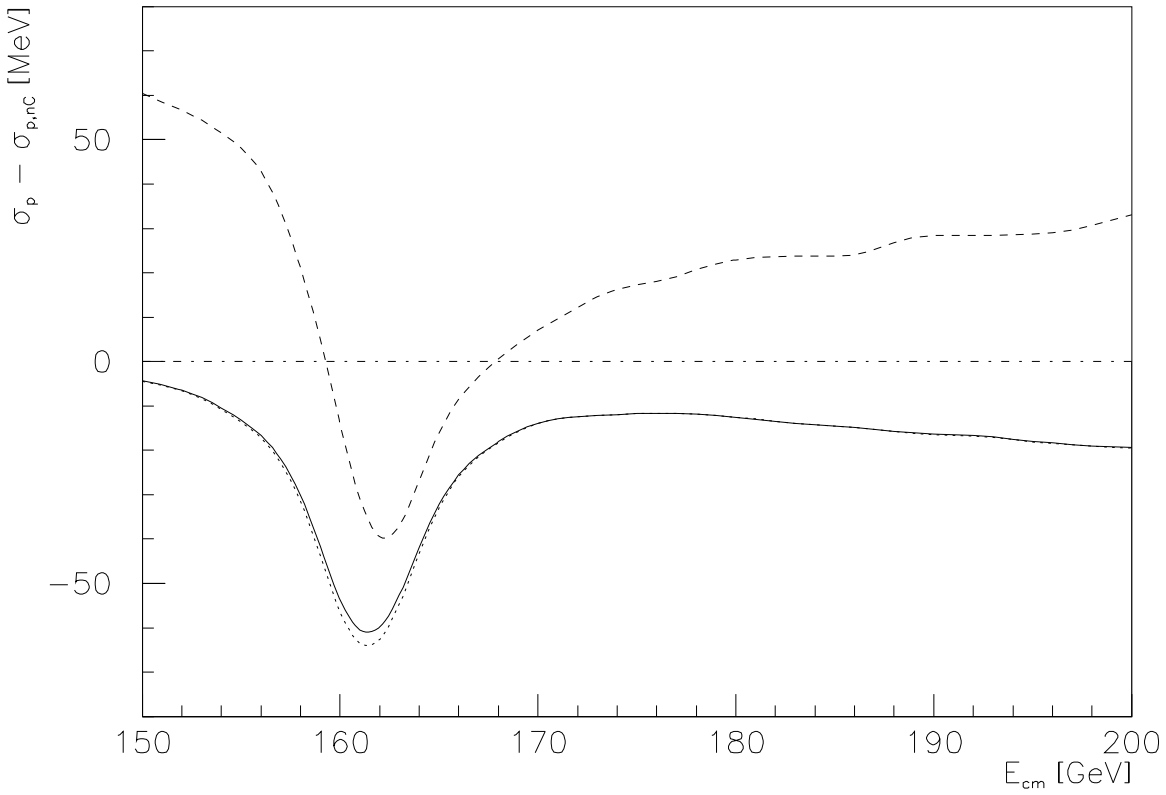

Figure 17

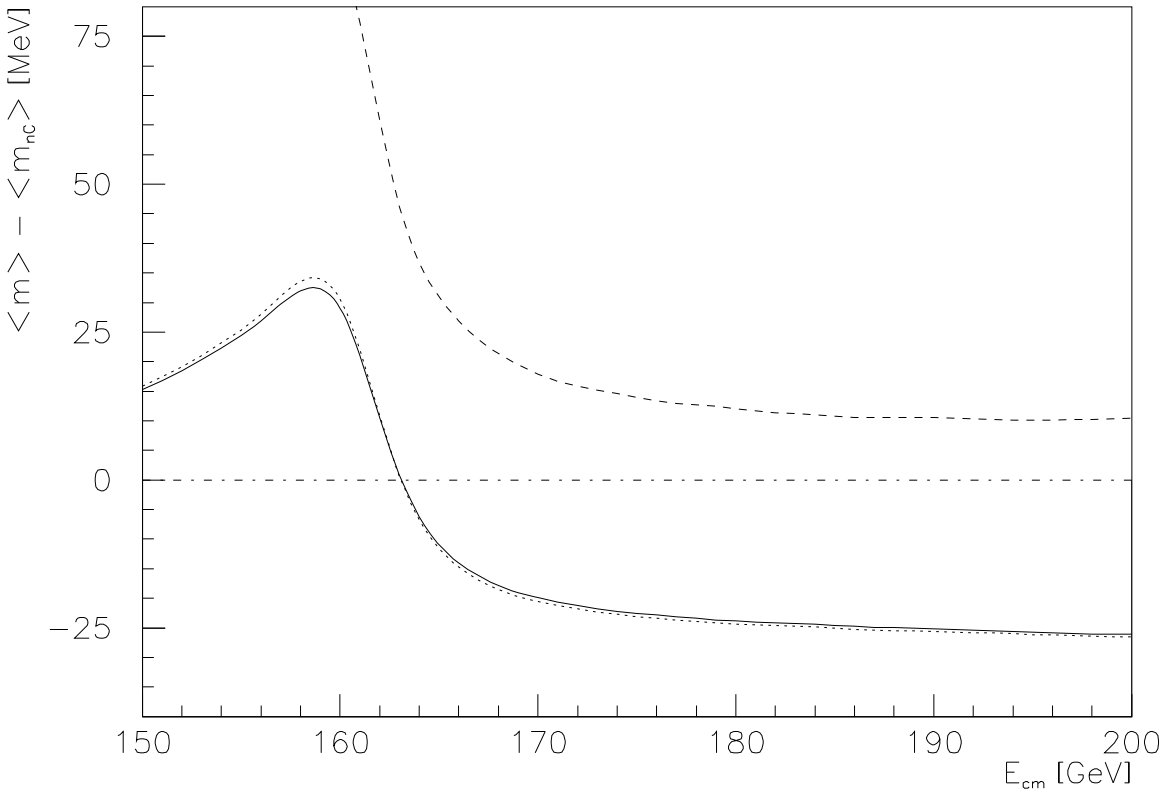

Figure 18

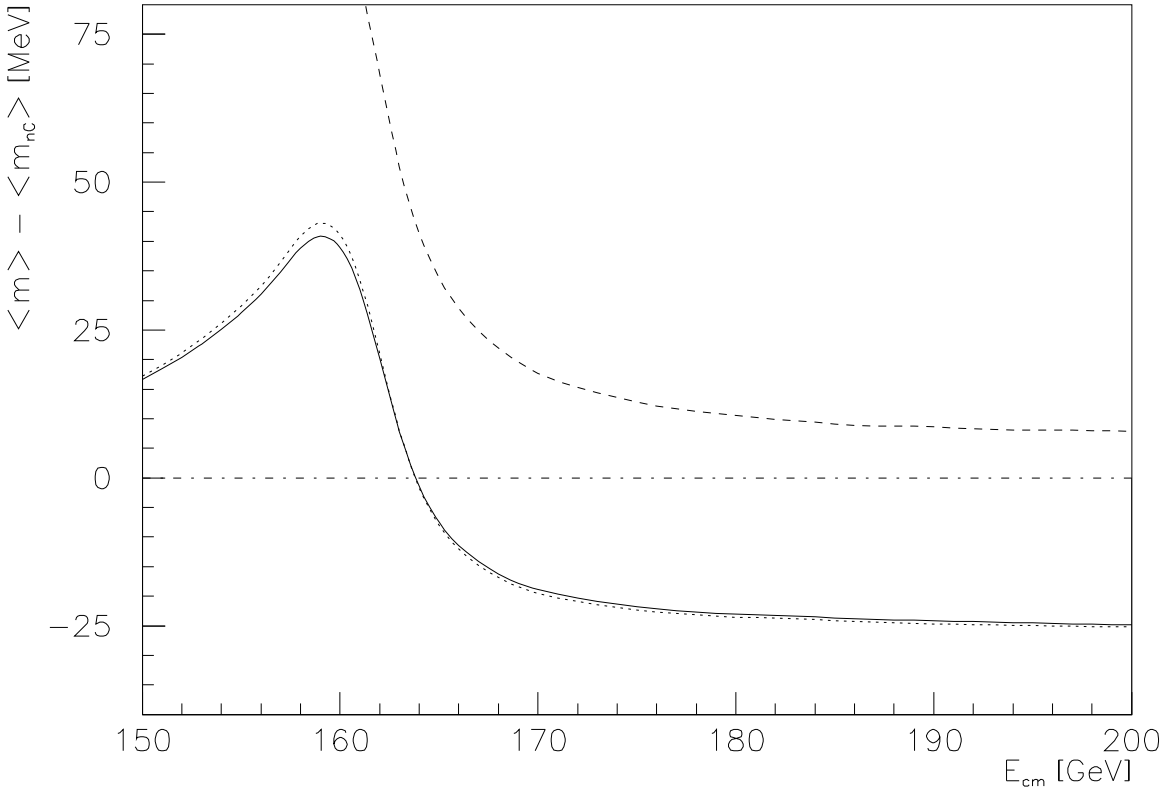

Figure 19

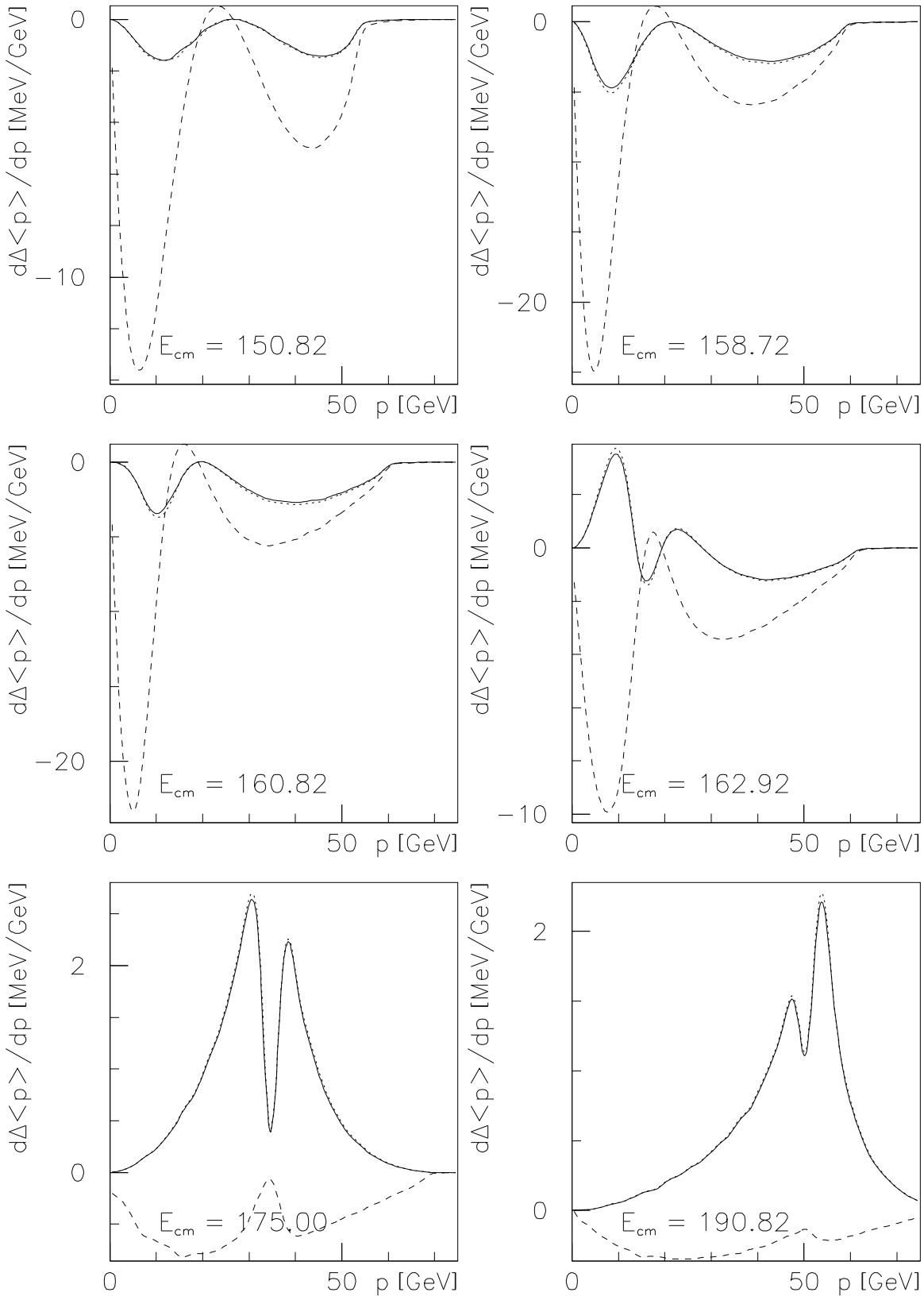
dΔ<p>/dp [MeV/GeV]
0
−10
E_{cm} = 150.82
0
50 p [GeV]
dΔ<p>/dp [MeV/GeV]
0
−20
E_{cm} = 158.72
0
50 p [GeV]
dΔ<p>/dp [MeV/GeV]
0
−20
E_{cm} = 160.82
0
50 p [GeV]
dΔ<p>/dp [MeV/GeV]
0
−10
E_{cm} = 162.92
0
50 p [GeV]
dΔ<p>/dp [MeV/GeV]
2
0
E_{cm} = 175.00
0
50 p [GeV]
dΔ<p>/dp [MeV/GeV]
2
0
E_{cm} = 190.82
0
50 p [GeV]

Figure 20

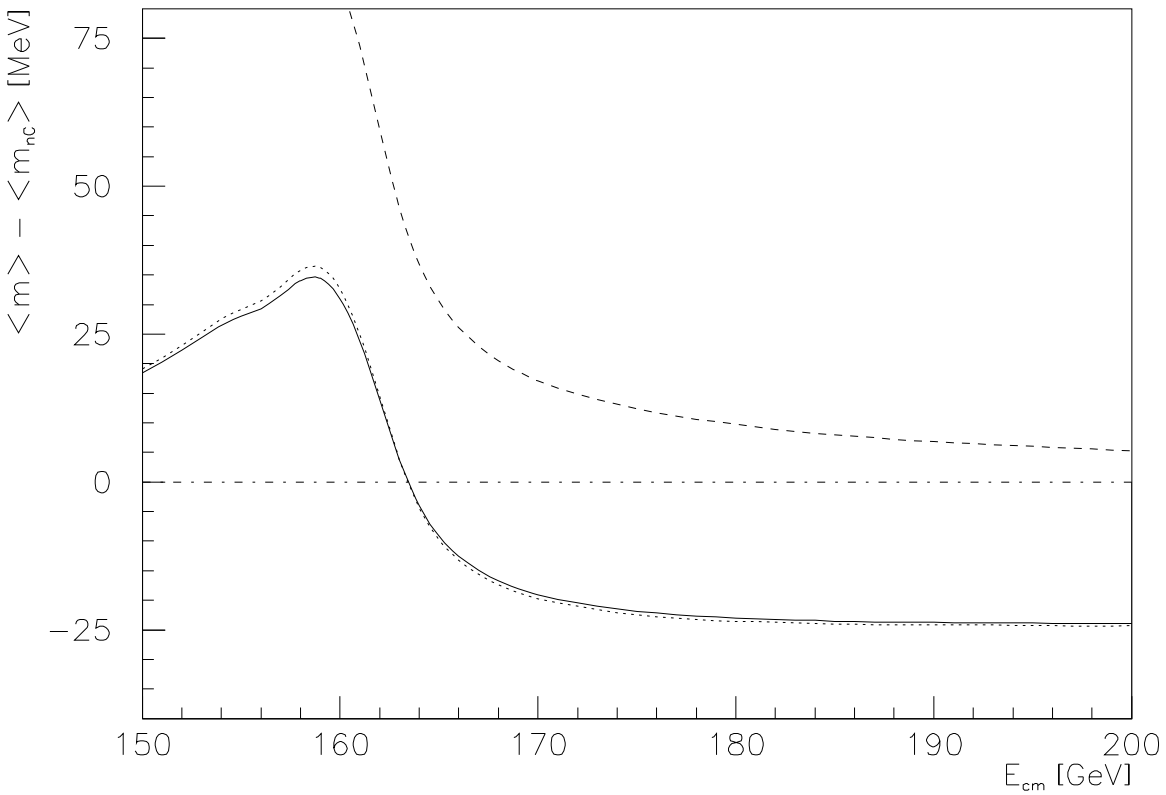

Figure 21

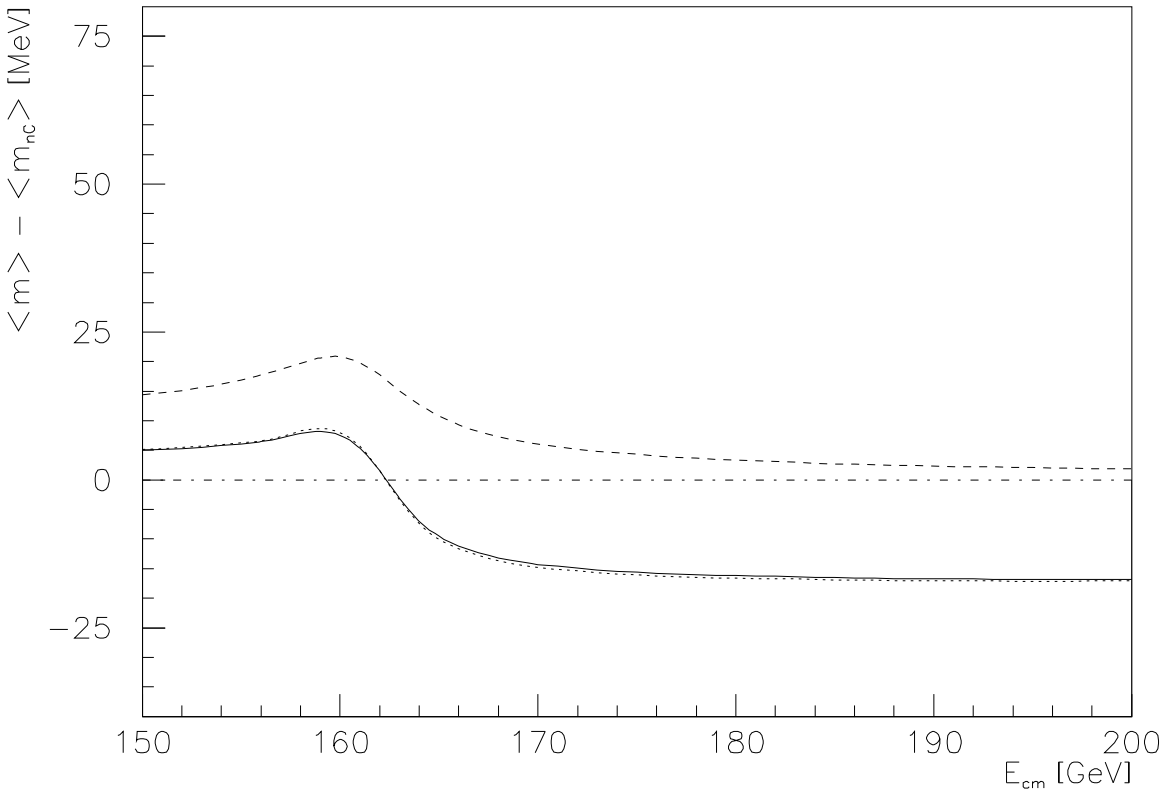

Figure 22

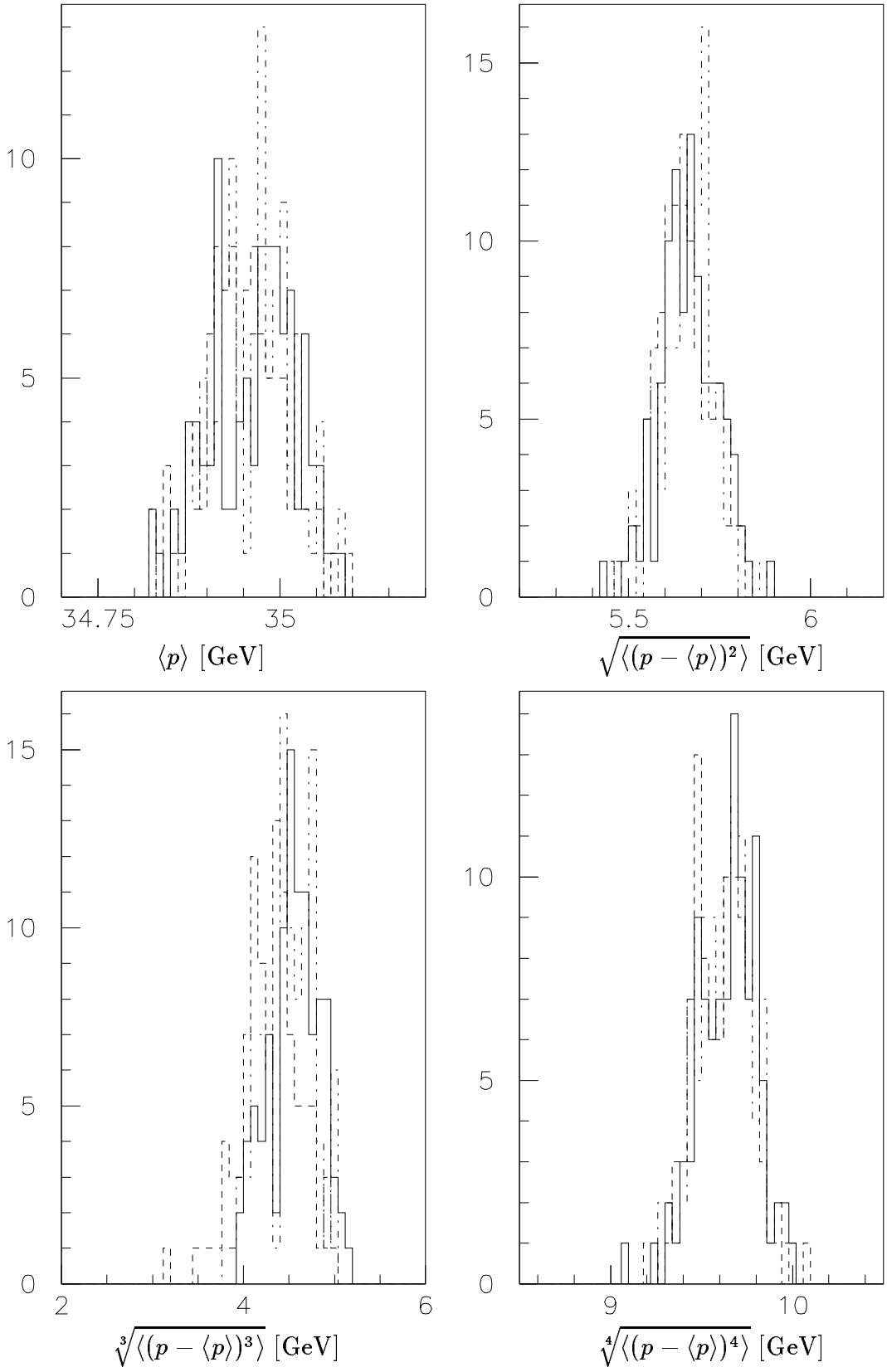
10
5
0
34.75
35
$\langle p \rangle$ [GeV]
15
10
5
0
5.5
6
$\sqrt{\langle (p - \langle p \rangle)^2 \rangle}$ [GeV]
15
10
5
0
2
4
6
$\sqrt[3]{\langle (p - \langle p \rangle)^3 \rangle}$ [GeV]
10
5
0
9
10
$\sqrt[4]{\langle (p - \langle p \rangle)^4 \rangle}$ [GeV]

Figure 23